Monthly Notices
of the
ROYAL ASTRONOMICAL SOCIETY

MNRAS **479,** 3232–3253 (2018)
Advance Access publication 2018 June 15

doi:10.1093/mnras/sty1581

Type II supernovae in low-luminosity host galaxies

C. P. Gutiérrez,[1⋆] J. P. Anderson,[2⋆] M. Sullivan,[1⋆] L. Dessart,[3] S. González-Gaitan,[4] L. Galbany,[5] G. Dimitriadis,[6] I. Arcavi,[7,8] F. Bufano,[9] T.-W. Chen,[10] M. Dennefeld,[11] M. Gromadzki,[12] J. B. Haislip,[13] G. Hosseinzadeh,[7,8] D. A. Howell,[7,8] C. Inserra,[1] E. Kankare,[14] G. Leloudas,[15] K. Maguire,[14] C. McCully,[7,8] N. Morrell,[16] F. Olivares E.,[17,18] G. Pignata,[19,17] D. E. Reichart,[13] T. Reynolds,[20] S. J. Smartt,[14] J. Sollerman,[21] F. Taddia,[21] K. Takáts,[17,19] G. Terreran,[22] S. Valenti[23] and D. R. Young[14]

Affiliations are listed at the end of the paper

Accepted 2018 June 7. Received 2018 June 7; in original form 2018 March 16

ABSTRACT

We present an analysis of a new sample of type II core-collapse supernovae (SNe II) occurring within low-luminosity galaxies, comparing these with a sample of events in brighter hosts. Our analysis is performed comparing SN II spectral and photometric parameters and estimating the influence of metallicity (inferred from host luminosity differences) on SN II transient properties. We measure the SN absolute magnitude at maximum, the light-curve plateau duration, the optically thick duration, and the plateau decline rate in the *V* band, together with expansion velocities and pseudo-equivalent-widths (pEWs) of several absorption lines in the SN spectra. For the SN host galaxies, we estimate the absolute magnitude and the stellar mass, a proxy for the metallicity of the host galaxy. SNe II exploding in low-luminosity galaxies display weaker pEWs of Fe II λ5018, confirming the theoretical prediction that metal lines in SN II spectra should correlate with metallicity. We also find that SNe II in low-luminosity hosts have generally slower declining light curves and display weaker absorption lines. We find no relationship between the plateau duration or the expansion velocities with SN environment, suggesting that the hydrogen envelope mass and the explosion energy are not correlated with the metallicity of the host galaxy. This result supports recent predictions that mass-loss for red supergiants is independent of metallicity.

Key words: supernovae: general – galaxies: general.

1 INTRODUCTION

Type II supernovae (SNe II) are the terminal explosions of massive (>8 $M_\odot$) stars that have retained a significant fraction of their hydrogen envelopes and, hence, have optical spectra that exhibit strong Balmer lines (Minkowski 1941). Initially, SNe II were separated into two groups: those with faster declining light curves were classified as SNe IIL, while those with a plateau in their light curves (a quasi-constant luminosity for a period of a few months) were classified as as SNe IIP (Barbon, Ciatti & Rosino 1979). This distinction has recently been refined with larger samples of events that show a continuum in their photometric properties (e.g. Anderson et al. 2014; Sanders et al. 2015). This continuum suggests that SNe II[1] events all come from the same progenitor population. The direct identification of the progenitors on pre-explosion images (Smartt 2015) has shown this population to be red supergiants (RSGs).

However, a significant diversity in the properties of SNe II is observed. Large samples of events have begun to provide some understanding of this diversity (e.g. Arcavi et al. 2012; Anderson et al. 2014; Faran et al. 2014a,b; Pejcha & Prieto 2015a,b; González-Gaitán et al. 2015; Valenti et al. 2016; Galbany et al. 2016; Rubin et al. 2016; Gutiérrez et al. 2017a,b). It has been found that SNe II with faster decline rates exhibit a shorter plateau duration (Anderson et al. 2014; Valenti et al. 2016; Gutiérrez et al. 2017b). In addition, they are brighter at 50 d from explosion and during the radioac-

⋆ E-mail: c.p.gutierrez-avendano@soton.ac.uk (CPG); janderso@eso.org (JPA); M.Sullivan@soton.ac.uk (MS)
† Einstein Fellow.
‡ Alexander von Humboldt Fellow.

[1]Throughout the remainder of the manuscript, we use SNe II to refer to all SNe which would historically have been classified as SN IIP or SN IIL. Type IIn, IIb, and 87A-like events are excluded from our analysis.

tive tail phase, and have broader spectral absorption features (e.g. Hamuy 2003; Pastorello et al. 2003; Faran et al. 2014b; Pejcha & Prieto 2015a,b; Gutiérrez et al. 2017b). These results suggest that the diversity is produced by differences in the progenitor and the explosion mechanisms (e.g. the amount of the hydrogen envelope mass, the explosion energy, the radius, metallicity, and mass-loss).

SNe II have been proposed as environmental metallicity probes. Dessart et al. (2013, 2014, hereafter D14) presented SN II spectral models produced from progenitors with different metallicities: 0.1, 0.4, 1, and 2 times solar metallicity ($Z_{\odot}$). With these models, they predict that the strength of the metal lines during the recombination phase should be related to the metallicity of the SN progenitor. They also note a lack of SNe II at metallicities below 0.4 $Z_{\odot}$, supporting the results of Stoll et al. (2013). Using a sample of 119 SNe II and gas-phase metallicity estimates derived from emission line measurements, Anderson et al. (2016, hereafter A16) confirmed this prediction by showing a correlation between gas-phase metallicity and SN II pseudo-equivalent-widths (pEWs) of the Fe II λ5018 line [pEW(Fe II 5018)]: SNe II exploding in higher metallicity galaxies have stronger iron lines in their spectra compared to those in lower metallicity environments. However, no trend was seen with any other SN II property, and A16 therefore concluded that progenitor metallicity likely plays only a minor role in driving SN II diversity. However, they noted that the range in host galaxy luminosity sampled was not particularly large ($-18 \gtrsim M_B^{\rm host} \gtrsim -22$).

This restricted range in host galaxy luminosity has now been overcome with new surveys that scan large areas of the sky without preference to the location of bright, nearby galaxies. Such searches have found new trends with respect to the ratios of different SN types as a function of galaxy luminosity (see Arcavi et al. 2010), but detailed studies of the properties of SNe II located in low-luminosity hosts are still generally lacking.

A recent exception is Taddia et al. (2016, hereafter T16), who analysed a further 39 SNe II taken from the (intermediate) Palomar Transient Factory sample of Rubin et al. (2016), extending the sample to lower metallicity with 18 events. These events showed smaller pEW(Fe II 5018), with a weak correlation between the inferred host galaxy metallicity (using an average luminosity–colour–metallicity relationship) and pEW(Fe II 5018). In addition, T16 showed that SNe II with brighter peak magnitudes tend to occur at lower metallicity.

This paper builds on these earlier studies, analysing a larger number of SNe II in low-luminosity hosts and their properties. Of particular interest is the duration of the 'plateau' phase in SN II light curves ($P_{\rm d}$). This has long been linked to the mass of the hydrogen-rich envelope of the progenitor star at the time of explosion (e.g. Popov 1993, and recent discussion in Gutiérrez et al. 2017b), as $P_{\rm d}$ is believed to be directly related to the time the hydrogen envelope takes to fully recombine. The hydrogen envelope mass is itself related to the mass-loss suffered by the progenitor star during its lifetime and the amount of hydrogen that has been fused into higher mass elements in the core. Given the metallicity dependence of mass-loss for hot single stars (e.g. Vink, de Koter & Lamers 2001; Mokiem et al. 2007), most stellar models predict a strong dependence of core-collapse SN type on progenitor metallicity (e.g. Heger et al. 2003; Chieffi & Limongi 2013). This metallicity dependence of mass-loss is also presumed to affect the hydrogen envelope mass retained by SN II progenitors, leading to a predicted dependence of the $P_{\rm d}$ on progenitor metallicity.

It should be noted, however, that the majority of the mass-loss suffered by a SN II progenitor will happen during the RSG phase, and currently there is no strong observational evidence that the strength of RSG mass-loss correlates with metallicity. A recent study by Chun et al. (2017) showed that metallicity dependence of mass-loss is only apparent when the Schwarzschild criterion for convection is employed; using the Ledoux criterion, the envelope mass at the epoch of explosion for SNe II was almost independent of progenitor metallicity. This result is supported by Goldman et al. (2017), who found no metallicity dependence of mass-loss for RSGs in the Large Magellanic Cloud (LMC) between half and twice solar metallicity. Within this context, observations of SNe II arising from a large range of environmental (and therefore progenitor) metallicity could be highly constraining for stellar models.

This paper presents 30 new SNe II in low-luminosity host galaxies. Using measurements of the SN photometric and spectroscopic properties, our aim is to further test the validity of using SNe II as metallicity indicators, and to constrain massive star models and SN II progenitors by searching for correlations of SN II parameters with host galaxy properties. The paper is organized as follows. In Section 2, we describe our sample and observations. The measurements are presented in Section 3, while the results and discussion are presented in Sections 4 and 5, respectively. We conclude in Section 6. Throughout, we assume a flat ΛCDM universe, with a Hubble constant of $H_0 = 70\ {\rm km\,s^{-1}\ Mpc^{-1}}$, and $\Omega_{\rm m} = 0.3$.

2 DATA SAMPLE AND OBSERVATIONS

In this paper, we present a new sample of 30 SNe II in low-luminosity host galaxies, and combine with a further 108 events sampling a range of host galaxy luminosities and taken from the literature (A16, Gutiérrez et al. 2017a, and references therein). Our new SNe II were selected so that they were (i) located in galaxies with an absolute magnitude in the B-band ($M_B^{\rm host}$) of $M_B^{\rm host} \gtrsim -18.5$mag, or were apparently hostless, and (ii) younger than 20 d post explosion. This absolute magnitude limit was chosen as it is around the brightness of the LMC, and because very few SN II were observed in the sample used by D14 with implied metallicities below that of the LMC. In this section, we present the data on the new sample of events, including their optical photometry and spectroscopy, and the data on their host galaxies.

2.1 SN sample

Observations for the new low-luminosity host sample of 30 objects are drawn from several sources. We took data on SNe II from the Public ESO Spectroscopic Survey for Transient Objects (PESSTO; Smartt et al. 2015, and the extended PESSTO, ePESSTO), which specifically targeted SNe II in faint host galaxies, and from the Las Cumbres Observatory (LCO; Brown et al. 2013) Supernova Key Project and the LCO Global Supernova Project. These events were generally observed photometrically with a 3 d cadence, and with spectral observations every few weeks. Finally, one additional SN II was detected and observed in 2009 by the CHilean Automated Supernova sEarch (CHASE; Pignata et al. 2009). Our comparison literature SNe II are taken from the various samples observed between 1986 and 2009 and compiled in Anderson et al. (2014). These comprise: the Cerro Tololo Supernova Survey (CTSS), the Calán/Tololo survey (CT; Hamuy et al. 1993), the Supernova Optical and Infrared Survey (SOIRS), the Carnegie Type II Supernova Survey (CATS) and the Carnegie Supernova Project (CSP-I; Hamuy et al. 2006). Table 1 gives the SN host galaxy information: recession velocity, $M_B^{\rm host}$ (used for the sample selection) and the reddening due to dust in our Galaxy ($E(B-V)_{\rm MW}$), as well as details of the discovery date and explosion epoch of each SN.

Table 1. SN II sample.

SN	Host Galaxy	Recession velocity (km s^{-1})	Host M_B type	$E(B-V)_{\rm MW}$ (mag)	Discovery date MJD	Source discovery	Discovery reference	Explosion epoch
SN2009lq	Anonymous	13 290[a]	–	0.027	55158.5	CHASE	CBET 2039	55 156.1[n](2.5)
ASASSN-14dq	UGC 11860	3 125	− 18.30	0.062	56847.0	ASAS-SN	ATEL 6301	56 841.0[n](5)
SN2014cw	PGC 68414	1 800	–	0.052	56899.0	MASTER	ATEL 6435	56 892.6[s](6)
ASASSN-14kp	GALEXASC J003952.48-380347.3	6 900	− 16.87	0.012	56974.0	ASAS-SN	ATEL 6736	56 971.6[n](2)
SN2015V	UGC 11000	1 369	− 18.50	0.034	57117.0	LOSS	ATEL 7345	57 113.0[n](4)
SN2015W	UGC 3617	3 984	− 18.62	0.123	57035.0	LOSS	CBET 4168	57 004.4[s](3)
SN2015aq	UGC 5015	1 650	− 16.51	0.015	57287.0	MASTER	ATEL 8077	57 253.9[s](6)
SN2015bm	Anonymous	4 500	–	0.026	57385.0	Blaz Mikuz	CBAT TOCP	57 384.1[s](9)
SN2015bs	Anonymous	8 100[a]	–	0.045	56925.6	CRTS	–	56 920.5[n](5)
ASASSN-15kz	IC 4303	2 405	− 18.06	0.053	57185.6	ASAS-SN	ATEL 7625	57 183.6[n](2)
ASASSN-15lx	ESO 047-G004	3 785	− 18.28	0.050	57199.6	ASAS-SN	ATEL 7719	57 198.0[n](0.5)
ASASSN-15oz	HIPASS J1919-33	2 078	–	0.080	57266.0	ASAS-SN	ATEL 7989	57 262.0[n](4)
ASASSN-15rp	GALEXASC J000337.23-343323.1	8 682	–	0.014	57298.5	ASAS-SN	ATEL 8199	57 296.5[n](1)
SN2016B	PGC 037392	1 287	− 16.48	0.019	57384.0	ASAS-SN	ATEL 8502	57 382.5[n](1.5)
SN2016O	2dFGRS N109Z338	3 000	− 15.58	0.034	57395.6	Pan-STARRS1	–	57 389.3[n](8)
SN2016X	UGC 8041	1 321	− 18.53	0.020	57406.6	ASAS-SN	ATEL 8566	57 406.0[n](0.6)
SN2016aqf	NGC 2101	1 204	− 17.66	0.049	57444.6	ASAS-SN	ATEL 8736	57 443.6[n](1)
SN2016ase	ESO 504-G9	4 380	− 17.75	0.042	57453.8	ASAS-SN	ATEL 8784	57 453.3[n](0.5)
SN2016blz	SDSS J154029.29+005437.4	3 517	− 17.56	0.090	57488.5	ASAS-SN	ATEL 8930	57 485.5[n](3)
SN2016dbm	Anonymous	18 900	–	0.056	57343.5	GaiaAlerts	TNS	57 336.0[n](7)
SN2016dpd	Anonymous	6 450[a]	–	0.077	57368.5	ASAS-SN	ATEL 8436	57 367.0[n](1.5)
SN2016drl	Anonymous	18 000[a]	–	0.069	57433.5	GaiaAlerts	TNS	57 434.0[c]
SN2016egz	GALEXASC J000403.88-344851.6	6 955	− 16.36	0.013	57590.5	ASAS-SN	ATEL 9262	57 588.5[n](2)
SN2016enk	UGC 9857	2 338	− 18.01	0.022	57600.5	ASAS-SN	ATEL 9305	57 598.5[n](2)
SN2016enp	SDSS J233425.10-063441.4	9 000	–	0.032	57601.5	ATLAS	ATEL 9318	57 590.2[n](11)
SN2016gsd	Anonymous	19 500[a]	–	0.082	57658.5	Koichi Itagaki	TNS	57 649.0[n](9.5)
SN2016hmq	2MASX J04250492-0733581	5 217	− 18.39	0.063	57685.5	Pan-STARRS1	ATEL 9686	57 674.0[s](5)
SN2016hpt	GALEXASC J215436.98-425103.9	7 800[a]	–	0.014	57686.5	ASAS-SN	ATEL 9697	57 685.0[n](1.5)
SN2017pn	Anonymous	4 200	–	0.120	57779.5	ATLAS	TNS	57 775.3[n](4)
SN2017vp	Anonymous	15 000	–	0.040	57779.5	Pan-STARRS1	TNS	57 760.0[s](6)
SN1986L	NGC 1559	1 305	− 21.34	0.026	46711.1	Robert Evans	IAUC 4260	46 708.0[n](3)
SN1990E	NGC 1035	1 241	− 19.27	0.022	47937.7	C. Pennypacker et al.	IAUC 4965	47 935.1[n](3)
SN1990K	NGC 0150	1 584	− 20.40	0.013	48037.3	Robert Evans	IAUC 5022	48 001.5[n](6)
SN1991al	2MASX J19422191-5506275	4 575[a]	− 21.18	0.054	48453.7	Marina Wischnjewsky	IAUC 5310	48 442.5[s](8)
SN1992af	ESO 340-G038	5 541	− 19.68	0.046	48802.8	Roberto Antezana	IAUC 5554	48 798.8[s](8)
SN1992am	MCG -01-04-039	14 397[a]	− 21.40	0.046	48829.8	Roberto Antezana	IAUC 5570	48 813.9[s](6)
SN1992ba	NGC 2082	1 185	− 17.99	0.051	48896.2	Robert Evans	IAUC 5625	48 884.9[s](7)
SN1993A	2MASX J07391822-6203095	8 790[a]	− 18.90	0.153	49004.6	Marina Wischnjewsky	IAUC 5693	48 995.5[n](9)
SN1993K	NGC 2223	2 724	− 20.85	0.056	49075.5	Williams, Martin	IAUC 5733	49 065.5[n](9)
SN1993S	2MASX J22522390-4018432	9 903	− 20.54	0.014	49133.7	Roberto Antezana	IAUC 5812	49 130.8[s](5)
SN1999br	NGC 4900	960	− 19.44	0.021	51281.0	LOSS	IAUC 7141	51 276.7[n](4)
SN1999ca	NGC 3120	2 793	− 20.39	0.096	51296.0	PARG	IAUC 7158	51 277.5[s](7)
SN1999cr	ESO 576-G034	6 069[a]	− 20.39	0.086	51249.7	Roberto Antezana	IAUC 7210	51 246.5[s](4)
SN1999eg	IC 1861	6 708	− 20.73	0.104	51455.5	Mark Armstrong	IAUC 7275	51 449.5[s](6)
SN1999em	NGC 1637	717	− 19.14	0.036	51481.0	LOSS	IAUC 7294	51 476.5[n](5)
SN2002ew	NEAT J205430.50-000822.0	8 975	–	0.091	52510.8	Nearby SN Factory	IAUC 7964	52 500.6[n](10
SN2002fa	NEAT J205221.51+020841.9	17 988	–	0.088	52510.8	Nearby SN Factory	IAUC 7967	52 502.5[s](8)
SN2002gd	NGC 7537	2 676	− 19.82	0.059	52552.7	Alain Klotz, et al.	IAUC 7986	52 551.5[s](4)
SN2002gw	NGC 922	3 084	–	0.017	52560.7	Takao Doi; Berto Monard	IAUC 7995	52 553.5[s](8)
SN2002hj	NPM1G +04.0097	7 080	− 17.98	0.102	52568.0	Nearby SN Factory	IAUC 8006	52 562.5[n](7)

Table 1 – *continued*

SN	Host Galaxy	Recession velocity (km s^{-1})	Host M_B type	$E(B-V)_{MW}$ (mag)	Discovery date MJD	Source discovery	Discovery reference	Explosion epoch
SN2002hx	PGC 023727	9 293	– 20.99	0.048	52589.7	SDSS	IAUC 8015	52 582.5^{n}(9)
SN2002ig	SDSS J013637.22+005524.9	23 100^{b}	–	0.034	52576.7	SDSS	IAUC 8020	52 570.5^{s}(5)
SN2003B	NGC 1097	1 272	– 21.42	0.024	52645.0	Robert Evans	IAUC 8042	52 613.5^{s}(11
SN2003bl	NGC 5374	4 377^{a}	–	0.024	52701.0	LOTOSS	IAUC 8086	52 696.5^{s}(4)
SN2003bn	2MASX J10023529-2110531	3 828	–	0.057	52698.0	Nearby SN Factory	IAUC 8088	52 694.5^{n}(3)
SN2003ci	UGC 6212	9 111	– 22.14	0.053	52720.0	LOTOSS	IAUC 8097	52 711.5^{n}(8)
SN2003cn	IC 849	5 433^{a}	– 20.61	0.019	52728.0	LOTOSS	IAUC 8101	52 717.5^{s}(4)
SN2003cx	NEAT J135706.53-170220.0	11 100	–	0.083	52730.0	Nearby SN Factory	IAUC 8105	52 725.5^{s}(5)
SN2003dq	MAPS-NGP O4320786358	13 800	– 17.52	0.016	52739.7	Nearby SN Factory	IAUC 8117	52 731.5^{n}(8)
SN2003E	MCG -4-12-004	4 470^{a}	– 17.99	0.043	52645.0	LOTOSS	IAUC 8044	52 629.5^{s}(8)
SN2003ef	NGC 4708	4 440^{a}	–	0.041	52770.7	LOTOSS	IAUC 8131	52 757.5^{s}(9)
SN2003eg	NGC 4727	4 388^{a}	– 22.26	0.046	52776.7	LOTOSS	IAUC 8134	52 764.5^{s}(5)
SN2003ej	UGC 7820	5 094	– 20.87	0.017	52779.7	LOTOSS	IAUC 8134	52 775.5^{n}(5)
SN2003fb	UGC 11522	5 262^{a}	– 20.89	0.162	52796.0	LOTOSS	IAUC 8143	52 772.5^{s}(10
SN2003gd	M74	657	– 20.58	0.062	52803.2	Robert Evans	IAUC 8150	52 755.5^{s}(9)
SN2003hd	MCG -04-05-010	11 850	– 21.73	0.011	52861.0	LOTOSS	IAUC 8179	52 855.9^{s}(5)
SN2003hk	NGC 1085	6 795	– 21.41	0.033	52871.6	Tom Boles; LOTOSS	CBET 41	52 866.8^{s}(4)
SN2003hl	NGC 772	2 475	– 22.39	0.064	52872.0	LOTOSS	IAUC 8184	52 868.5^{n}(5)
SN2003hn	NGC 1448	1 170	– 21.06	0.013	52877.2	Robert Evans	IAUC 8186	52 866.5^{n}(10
SN2003ho	ESO 235-G58	4 314	– 19.85	0.034	52851.9	Berto Monard	IAUC 8186	52 848.5^{s}(7)
SN2003ib	MCG -04-48-15	7 446	– 20.78	0.043	52898.7	LOTOSS	IAUC 8201	52 891.5^{n}(8)
SN2003ip	UGC 327	5 403	– 19.47	0.058	52913.7	LOTOSS	IAUC 8214	52 896.5^{s}(4)
SN2003iq	NGC 772	2 475	– 22.39	0.064	52921.5	JM Llapasset	CBET 48	52 919.5^{n}(2)
SN2003T	UGC 4864	8 373	– 20.72	0.028	52665.0	Mike Schwartz, LOTOSS	IAUC 8058	52 654.5^{n}(10)
SN2004dy	IC 5090	9 352	– 21.79	0.045	53242.5	LOSS	IAUC 8395	53 240.5^{n}(2)
SN2004ej	NGC 3095	2 723	– 21.55	0.061	53258.5	Berto Monard	IAUC 8405	53 223.9^{s}(9)
SN2004er	MCG -01-7-24	4 411	– 20.35	0.023	53274.0	LOSS	IAUC 8412	53 271.8^{n}(2)
SN2004fb	ESO 340-G7	6 100	– 20.88	0.056	53286.2	Lulin Observatory	IAUC 8420	53 258.6^{s}(7)
SN2004fc	NGC 701	1 831	– 19.51	0.023	53295.2	LOSS	IAUC 8422	53 293.5^{n}(1)
SN2004fx	MCG -02-14-3	2 673	–	0.090	53307.0	LOSS	IAUC 8431	53 303.5^{n}(4)
SN2005af	NGC 4945	563	– 20.54	0.156	53409.7	Ceamig	IAUC 8482	53 320.8^{s}(17)
SN2005an	ESO 506-G11	3 206	– 18.62	0.083	53432.7	LOSS	CBET 113	53 431.8^{s}(6)
SN2005dk	IC 4882	4 708	– 19.74	0.043	53604.0	Tenagra Observatory	IAUC 8586	53 601.5^{s}(6)
SN2005dn	NGC 6861	2 829	– 21.03	0.048	53609.5	BRASS	IAUC 8589	53 602.6^{s}(6)
SN2005dt	MCG -03-59-6	7 695	– 20.94	0.025	53614.7	LOSS	CBET 213	53 605.6^{n}(9)
SN2005dw	MCG -05-52-49	5 269	– 21.12	0.020	53612.7	LOSS	CBET 219	53 603.6^{n}(9)
SN2005dx	MCG -03-11-9	8 012	– 20.75	0.021	53623.0	LOSS	CBET 220	53 611.8^{s}(7)
SN2005dz	UGC 12717	5 696	– 19.85	0.072	53623.7	Tim Puckett	CBET 222	53 619.5^{n}(4)
SN2005es	MCG +01-59-79	11 287	– 21.10	0.076	53643.7	LOSS	IAUC 8608	53 638.7^{n}(5)
SN2005J	NGC 4012	4 183	– 20.41	0.025	53387.0	Tenagra Observatory	IAUC 8467	53 379.8^{s}(7)
SN2005K	NGC 2923	8 204	– 20.25	0.035	53386.0	Tenagra Observatory	IAUC 8468	53 369.8^{s}(8)
SN2005me	ESO 244-31	6 726	– 21.41	0.022	53728.2	Berto Monard	CBET 333	53 717.9^{s}(10)
SN2005Z	NGC 3363	5 766	– 20.52	0.025	53402.0	LOSS	IAUC 8476	53 396.7^{n}(6)
SN2006ai	ESO 005-G009	4 571^{a}	– 19.22	0.113	53784.0	Tenagra Observatory	CBET 406	53 781.6^{s}(5)
SN2006bc	NGC 2397	1 363	– 20.89	0.181	53819.1	Perth Observatory	CBET 446	53 815.5^{n}(4)
SN2006be	IC 4582	2 145	– 18.62	0.026	53819.0	LOSS	CBET 449	53 802.8^{s}(9)
SN2006bl	MCG +02-40-9	9 708	– 21.04	0.045	53829.5	Tom Boles	CBET 462	53 822.7^{s}(10)
SN2006it	NGC 6956	4 650	– 21.10	0.087	54009.5	LOSS	CBET 660	54 006.5^{n}(3)
SN2006iw	2MASX J23211915+0015329	9 226	– 18.74	0.044	54011.5	SDSS	CBET 663	54 010.7^{n}(1)
SN2006ms	NGC 6935	4 543	– 21.34	0.031	54046.2	Berto Monard	CBET 725	54 028.5^{s}(6)
SN2006qr	MCG -02-22-023	4 350	– 20.24	0.040	54070.0	LOSS	CBET 766	54 062.8^{n}(7)
SN2006Y	anon	10 074^{b}	– 16.32	0.115	53770.0	Tenagra Observatory	IAUC 8668	53 766.5^{n}(4)
SN2007aa	NGC 4030	1 465	– 21.17	0.023	54149.7	Takao Doi	CBET 848	54 126.7^{s}(8)

Table 1 – *continued*

SN	Host Galaxy	Recession velocity (km s^{-1})	Host M_B type	$E(B-V)_{\rm MW}$ (mag)	Discovery date MJD	Source discovery	Discovery reference	Explosion epoch
SN2007ab	MCG -01-43-2	7 056	– 21.26	0.235	54150.7	Berto Monard	CBET 851	54 123.9^{s}(10)
SN2007av	NGC 3279	1 394	– 20.19	0.032	54180.2	Ron Arbour	CBET 901	54 173.8^{s}(5)
SN2007hm	SDSS J205755.65-072324.9	7 540	– 18.50	0.059	54343.7	Nearby SN Factory	CBET 1050	54 336.6^{s}(6)
SN2007il	IC 1704	6 454	– 20.87	0.042	54354.0	LOSS	CBET 1062	54 349.8^{n}(4)
SN2007it	NGC 5530	1 193	– 19.59	0.103	54357.5	Robert Evans	CBET 1065	54 348.5^{n}(1)
SN2007oc	NGC 7418	1 450	– 19.86	0.014	54396.5	CHASE	CBET 1114	54 388.5^{n}(3)
SN2007sq	MCG -03-23-5	4 579	– 22.22	0.183	54443.0	LOSS	CBET 1170	54 422.8^{s}(6)
SN2007W	NGC 5105	2 902	– 20.91	0.045	54146.5	Berto Monard	CBET 844	54 130.8^{s}(7)
SN2007X	ESO 385-G32	2 837	– 20.45	0.060	54146.5	Berto Monard	CBET 844	54 143.5^{s}(5)
SN2007Z	PGC 016993	5 277	– 22.84	0.525	54148.7	LPL	CBET 847	54 135.6^{s}(5)
SN2008ag	IC 4729	4 439	– 21.47	0.074	54499.5	Berto Monard	CBET 1252	54 477.9^{s}(8)
SN2008aw	NGC 4939	3 110	– 22.29	0.036	54528.0	LOSS; Robert Evans	CBET 1279	54 517.8^{n}(10)
SN2008bh	NGC 2642	4 345	– 20.93	0.020	54549.0	LOSS; CHASE	CBET 1311	54 543.5^{n}(5)
SN2008bk	NGC 7793	227	– 18.49	0.017	54550.7	Berto Monard	CBET 1315	54 540.9^{s}(8)
SN2008bm	CGCG 071-101	9 563	– 19.98	0.023	54554.7	CRTS	CBET 1320	54 522.8^{s}(6)
SN2008bp	NGC 3095	2 723	– 20.18	0.061	54558.7	CHASE	CBET 1326	54 551.7^{n}(6)
SN2008br	IC 2522	3 019	– 20.86	0.083	54564.2	Berto Monard	CBET 1332	54 555.7^{n}(9)
SN2008bu	ESO 586-G2	6 630	– 21.60	0.376	54574.0	LOSS	CBET 1341	54 566.8^{s}(7)
SN2008F	MCG -01-8-15	5 506	– 20.33	0.044	54477.5	T. Puckett and G. Sostero	CBET 1207	54 469.6^{s}(6)
SN2008ga	LCSB L0250N	4 639	–	0.582	54734.0	CRTS	CBET 1526	54 711.5^{s}(7)
SN2008gi	CGCG 415-004	7 328	– 20.01	0.060	54752.0	LOSS	CBET 1539	54 742.7^{n}(9)
SN2008gr	IC 1579	6 831	– 20.55	0.012	54768.7	T. Puckett and R. Gagliano	CBET 1557	54 769.6^{s}(6)
SN2008H	ESO 499- G 005	4 287	– 21.54	0.057	54481.0	LOSS	CBET 1210	54 432.8^{s}(8)
SN2008ho	NGC 922	3 082	– 20.81	0.017	54796.5	CHASE	CBET 1587	54 792.7^{n}(5)
SN2008if	MCG -01-24-10	3 440	– 20.48	0.029	54812.7	CHASE	CBET 1619	54 807.8^{n}(5)
SN2008il	ESO 355-G4	6 276	– 20.60	0.015	54827.7	CHASE	CBET 1634	54 825.6^{n}(3)
SN2008in	NGC 4303	1 566	– 20.36	0.020	54827.2	Koichi Itagaki	CBET 1636	54 825.4^{n}(2)
SN2008M	ESO 121-26	2 267	– 20.38	0.040	54480.7	BRASS	CBET 1214	54 471.7^{n}(9)
SN2008W	MCG -03-22-7	5 757	– 20.60	0.086	54502.7	LOSS	CBET 1238	54 483.8^{s}(8)
SN2009aj	ESO 221- G 018	2 883	– 19.23	0.130	54887.0	CHASE	CBET 1704	54 880.5^{n}(7)
SN2009ao	NGC 2939	3 339	– 20.67	0.034	54895.0	CHASE; Tim Puckett et al.	CBET 1711	54 890.7^{n}(4)
SN2009au	ESO 443-21	2 819	– 20.08	0.081	54902.0	CHASE	CBET 1719	54 897.5^{n}(4)
SN2009bu	NGC 7408	3 494	– 20.83	0.022	54916.2	CROSS	CBET 1740	54 901.9^{s}(8)
SN2009bz	UGC 9814	3 231	– 19.35	0.035	54920.0	LOSS	CBET 1748	54 915.8^{n}(4)
SN2009N	NGC 4487	1 034	– 20.28	0.019	54856.3	Koichi Itagaki	CBET 1670	54 846.8^{s}(5)

Note. SNe and host galaxy information. Columns: (1) SN name; (2) galaxy name; (3) the host galaxy heliocentric recession velocity. These are taken from the Nasa Extragalactic Database (NED; http://ned.ipac.caltech.edu/) unless indicated by a superscript (sources in table notes); (4) host galaxy absolute *B*-band magnitudes (taken from the LEDA database:;http://leda.univ-lyon1.fr/); (5) the reddening due to dust in our Galaxy (Schlafly & Finkbeiner 2011) taken from NED; (6) discovery date; (7) source of discovery: CHilean Automatic Supernovas sEarch (CHASE; http://www.das.uchile.cl/proyectoCHASE/), All-Sky Automated Survey for Supernovae (ASAS-SN; http://www.astronomy.ohio-state.edu/), MASTER Global Robotic Net (http://observ.pereplet.ru/), Lick Observatory Supernova Search (LOSS; http://w.astro.berkeley.edu/bait/kait.html), Catalina Real-Time Transient Survey (CRTS; http://nesssi.cacr.caltech.edu/CRTS/), Optical Gravitational Lensing Experiment (OGLE-IV), Transient Detection System (http://ogle.astrouw.edu.pl/ogle4/transients/2015/transients.html), Pan-STARRS1 (https://panstarrs.stsci.edu/), Gaia Photometric Science Alerts (GaiaAlerts; http://gsaweb.ast.cam.ac.uk/alerts/), ATLAS (http://fallingstar.com/home.php); Perth Astronomical Research Group (PARG; http://www.parg.asn.au/); Nearby Supernova Factory (SNFactory; https://snfactory.lbl.gov/); Alain Klotz (http://alain.klotz.free.fr/snalert/); Takao Doi (http://iss.jaxa.jp/en/astro/biographies/doi/index.html); Sloan Digital Sky Survey Collaboration (SDSS; http://www.sdss.org/collaboration/); Lick Observatory and Tenagra Observatory Supernova Search (LOTOSS; http://w.astro.berkeley.edu/bait/lotoss.html); Berto Monard (http://assa.saao.ac.za/about/awards/gill-medal/berto-monard-awarded-2004-gill-medal/); Tom Boles (http://www.coddenhamobservatories.org/); Lulin Observatory (http://www.lulin.ncu.edu.tw/); CEAMIG/REA Supernovae Search (http://www.ceamig.org.br/); Tenagra Observatory (http://www.tenagraobservatories.com/); Brazilian Supernovae Search (BRASS; http://brass.astrodatabase.net/index.htm); Perth Observatory (https://www.wa.gov.au/perthobs/); Ron Arbour (http://mstecker.com/pages/apparbour.htm); Lunar and Planetary Laboratory (LPL; https://www.lpl.arizona.edu/); Col Druscié Remore Observatory Supernovae Search (CROSS; http://www.cortinastelle.it/snindex.htm); (8) discovery reference; (9) explosion epoch. They are estimated using the SN non-detection or through the spectral matching. More details can be found in Gutiérrez et al. (2017a).

[a] Redshift obtained from the SN spectrum.

[b] Taken from the Asiago supernova catalogue: http://graspa.oapd.inaf.it/.

[c] Discovery epoch.

[s] Explosion epoch estimation through spectral matching.

[n] Explosion epoch estimation from SN non-detection.

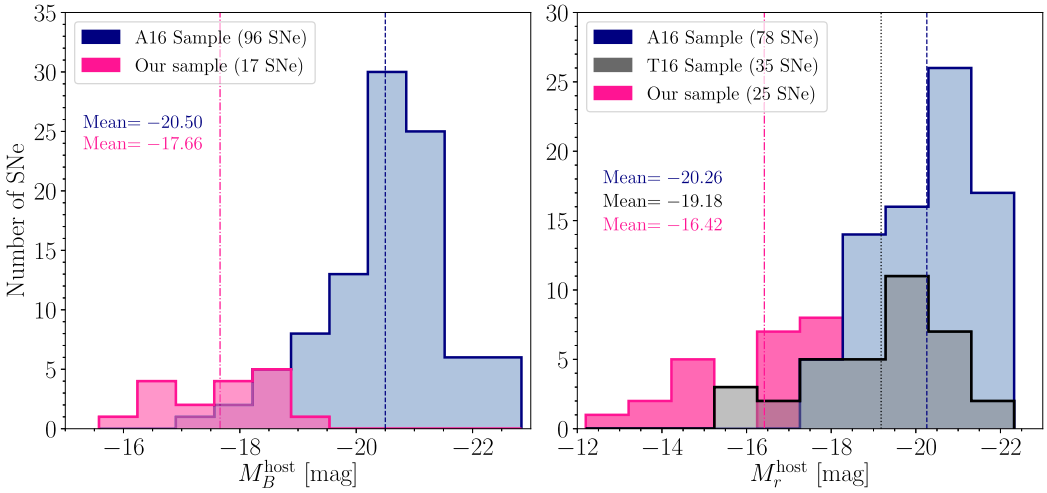

Figure 1. Distribution of the host galaxy absolute magnitudes for our sample (magenta), and for the A16 (blue) and T16 (black) samples. The left-hand panel shows the distribution of $M_B^{\rm host}$, and the right-hand panel the distribution of $M_r^{\rm host}$. The vertical lines indicate the mean for each sample (dashed: A16, dotted: T16, and dot–dashed: our sample). Note that not all of our 30 SNe II have host information in both filters (see Section 2.2 for further details).

In Fig. 1, we present the $M_B^{\rm host}$ and $M_r^{\rm host}$ distributions of our sample in comparison to A16 and T16. Our 30 new SNe extend the host galaxy luminosity distribution to fainter hosts, with a mean $M_r^{\rm host} = -16.42 \pm 0.39$ mag (cf. $M_r^{\rm host} = -20.26 \pm 0.14$ mag in A16, and $M_r^{\rm host} = -19.18 \pm 0.27$ mag in T16).

2.1.1 *Photometry*

Optical photometry was acquired for 29 of the 30 new low-luminosity host SNe II. The light curves of 24 SNe II were obtained by LCO, either as part of PESSTO, or as part of the LCO key projects, and reduced following the prescriptions described by Firth et al. (2015). 21 of these SNe were observed in *BVgri* filters, while the remaining four in *gri*. SN 2017vp was observed in the $g'r'i'z'JHK$ bands with the Gamma-Ray Burst Optical/Near-Infrared Detector (GROND; Greiner et al. 2008), at the 2.2-m MPG telescope at the European Southern Observatory (ESO) La Silla Observatory in Chile. The images were reduced with the GROND pipeline (Krühler et al. 2008), which applies de-bias and flat-field corrections, stacks images and provides an astrometric calibration. SN 2015bs was observed in *BVri* using the Swope telescope at the Las Campanas Observatory. The reduction procedure is presented in Anderson et al. (2018). SN 2009lq, ASASSN-14kp, and SN 2014cw were observed in *BVRI* with the PROMPT telescopes located at Cerro Tololo Inter-american Observatory. SN 2009lq was, in addition, observed with the TRAPPIST telescope at La Silla. The reduction of the images of these three SNe were performed following standard procedures (including bias, dark, and flat-field corrections), and calibrated using observations of standard-star fields (Landolt 1992, 2007; Smith et al. 2002). ASASSN-15rp has no photometric information. Details of the literature sample can be found in Anderson et al. (2014).

Table 2 presents a summary of all the observations obtained for the new low-luminosity host SNe II in our sample. The photometric data for SN 2016X and SN 2015bs are presented by Huang et al. (2018) and Anderson et al. (2018), respectively, while the data for ASASSN-14dq and SN 2015W were published in Valenti et al. (2016). Published data have been re-reduced and calibrated here for homogeneity within sample. Data (both photometric and spectroscopic) for ASASSN-15oz will be presented in a separate study by Bostroem (in preparation), for SN 2016B in Rui et al. (in preparation), for SN 2016blz in Johansson et al. (in preparation), for SN 2016dbm in Terreran et al. (in preparation), for SN 2016egz in Hiramatsu et al. (in preparation), for SN 2016enp in Reynolds et al. (in preparation), and for SN 2016gsd in Reynolds et al. (in preparation). Photometry and spectroscopy for the remaining unpublished SNe in the sample will be presented in a future data paper.

Throughout the paper, all magnitudes in our sample have been corrections for Milky Way extinction taken from Schlafly & Finkbeiner (2011). *K*-corrections were not applied because at low redshift the results are not affected. See Anderson et al. (2014) for more details.

2.1.2 *Spectroscopy*

In this paper, we make use of spectroscopic measurements at (or close to) 50 d after the SN explosion. These spectra come from a range of difference sources. Details of the instruments used for the spectral observations of the new sample are listed in Table 2, and all spectra from which we make the +50 d measurements in this paper are available through the WISeREP[2] archive (Yaron & Gal-Yam 2012). Spectroscopic data for SN 2015bs is presented in Anderson et al. (2018), and for SN 2016X in Huang et al. (2018). The PESSTO spectra up to May 2016 can also be retrieved from the ESO Science Archive Facility as Phase 3 data products.[3]

Spectroscopic observations were performed with the ESO Faint Object Spectrograph and Camera (EFOSC; Buzzoni et al. 1984) at the 3.5-m ESO New Technology Telescope (NTT), and the twin FLOYDS spectrographs on the Faulkes Telescope South (FTS) and the Faulkes Telescope North (FTN). The NTT spectra were reduced using the PESSTO pipeline (Smartt et al. 2015), while the FLOYDS data were reduced using the PYRAF-based `floydsspec` pipeline. Data for SN 2014cw were acquired with the Low Resolution Spectrograph (LRS) at the 3.6-m Telescopio Nazionale Galileo (TNG), the Ohio State Multi-Object Spectrograph (OSMOS) at the 2.4-m Hiltner Telescope, and the Goodman Spectrograph at the SOAR

[2] http://wiserep.weizmann.ac.il/home
[3] See http://www.pessto.org for access instructions.

Table 2. Observation details.

SN	Photometry source	Filters	Photometry coverage (d)	# Points	Spectroscopic[a] source	Spectra coverage (d)	# Spectra	Source of Spectra around 50 d
SN2009lq	PROMPT1,3,5	*BVRI*	140	17	LDSS3+WFCCD	120	2	–
ASASSN-14dq	LCO	*BVgri*	290[a]	40	FLOYDS	96	5	–
SN2014cw	PROMPT1,3,5	*BVRI*	350	8	EFOSC2+LRS+GS+OSMOS	114	4	GS
ASASSN-14kp	PROMPT1,3,5	*BVRI*	35	18	EFOSC2+WFCCD	76	10	EFOSC2
SN2015V	LCO	*BVgri*	210	28	FLOYDS	215	13	FLOYDS
SN2015W	LCO	*BVgri*	120	58	FLOYDS	96	13	FLOYDS
SN2015aq	LCO	*BVgri*	390[b]	42	FLOYDS	276	15	FLOYDS
SN2015bm	LCO	*gri*	140	30	EFOSC2	109	11	EFOSC2
SN2015bs	CSP II	*BVri*	80	16	EFOSC2	81	8	EFOSC2
ASASSN-15kz	LCO	*BVgri*	90	30	FLOYDS	82	8	FLOYDS
ASASSN-15lx	LCO	*BVgri*	340[c]	62	FLOYDS	150	17	FLOYDS
ASASSN-15oz	LCO	*BVgri*	400[d]	73	EFOSC2+FLOYDS	390	21	FLOYDS
ASASSN-15rp	–	–	–	–	EFOSC2	77	3	EFOSC2
SN2016B	LCO	*BVgri*	510[e]	63	EFOSC2+FLOYDS	390	30	EFOSC2
SN2016O	LCO	*gri*	110	14	EFOSC2	94	8	EFOSC2
SN2016X	LCO	*BVgri*	190	46	EFOSC2+FLOYDS	141	29	EFOSC2
SN2016aqf	LCO	*BVgri*	300[f]	33	EFOSC2+FLOYDS	326	29	EFOSC2
SN2016ase	LCO	*BVgri*	150	45	EFOSC2+FLOYDS	147	16	FLOYDS
SN2016blz	LCO	*BVgri*	150	34	FLOYDS	143	14	FLOYDS
SN2016dbm	LCO	*BVgri*	110	25	EFOSC2	107	18	EFOSC2
SN2016dpd	LCO	*BVgri*	130	23	FLOYDS	53	8	FLOYDS
SN2016drl	LCO	*gri*	80	10	EFOSC2	59	7	EFOSC2
SN2016egz	LCO	*BVgri*	300[g]	50	EFOSC2+FLOYDS	179	34	EFOSC2
SN2016enk	LCO	*BVgri*	257[h]	28	FLOYDS	190	8	FLOYDS
SN2016enp	LCO	*gri*	150	22	EFOSC2	104	11	EFOSC2
SN2016gsd	LCO	*BVgri*	90	20	EFOSC2+FLOYDS	110	9	EFOSC2
SN2016hmq	LCO	*BVgri*	110	18	EFOSC2	100	8	EFOSC2
SN2016hpt	LCO	*BVgri*	40	6	EFOSC2	59	3	EFOSC2
SN2017pn	LCO	*BVgri*	70	13	EFOSC2	91	5	EFOSC2
SN2017vp	GROND	$g'r'i'z'JHK$	110	12	EFOSC2	50	4	EFOSC2

Note. LDSS3: Low Dispersion Survey Spectrograph at the Magellan Clay 6.5-m telescope; WFCCD: Wide Field CCD Camera at the 2.5-m du Pont Telescope; FLOYDS: FLOYDS spectrographs on the Faulkes Telescope South (FTS) and the Faulkes Telescope North (FTN); EFOSC2: ESO Faint Object Spectrograph and Camera at the 3.5-m ESO New Technology Telescope (NTT); LRS: Low Resolution Spectrograph at the 3.6m Telescopio Nazionale Galileo (TNG); GS**:** Goodman Spectrograph at the SOAR 4.1-m telescope; OSMOS: Ohio State Multi-Object Spectrograph at the 2.4-m Hiltner Telescope. Note that ASASSN-15rp does not have Photometric information.

[a] Break in the observations for ∼140 d.
[b] Break in the observations for ∼150 d.
[c] Break in the observations n for ∼150 d.
[d] Break in the observations for ∼100 d.
[e] Break in the observations for ∼130 d.
[f] Break in the observations for ∼70 d.
[g] Break in the observations for ∼100 d.
[h] Break in the observations for ∼69 d.

4.1-m telescope. For SN 2009lq, two spectra were obtained with the Wide Field CCD Camera (WFCCD) at the 2.5-m du Pont Telescope and the Low Dispersion Survey Spectrograph (LDSS3) on the Magellan Clay 6.5-m telescope at Las Campanas Observatory. For ASASSN-14kp, one spectrum was obtained with WFCCD. The reductions for LRS, TNG, OSMOS, Goodman, WFCCD, and LDSS3 spectra were performed using the standard routines (bias subtraction, flat-field correction, 1D extraction, and wavelength calibration). Details on the literature spectra are presented by Gutiérrez et al. (2017a).

2.2 Host galaxy data

Photometry for the SN host galaxies in the *ugriz* filters were collected from the Sloan Digital Sky Survey (SDSS) Data Release 13[4] (Albareti et al. 2017) and the Pan-STARRS1[5] (Flewelling et al. 2016; Chambers et al. 2016) data archive. In addition, *B*-band photometry (used in our initial SN selection for spectroscopic and photometric follow-up) was collected from the HyperLEDA[6] (Makarov et al. 2014) database. For SN 2015bs, $M_r^{\rm host}$ was obtained from Anderson et al. (2018), while for SN 2009lq, ASASSN-15oz, ASASSN-15rp, and SN 2016drl, where no host galaxy is visible, we determine an upper limit on the luminosity of the host using a circular aperture centred on the SN location. The host galaxy magnitudes can be found in Table 3.

[4] http://skyserver.sdss.org/dr13/en/home.aspx
[5] https://panstarrs.stsci.edu/
[6] http://leda.univ-lyon1.fr/

Table 3. Host galaxy information.

SN	Host M_B (mag)	Host M_u (mag)	Host M_g (mag)	Host M_r (mag)	Host M_i (mag)	Host M_z (mag)	Log($M_{\rm stellar}$) ($M_\odot$)
SN2009lq	–	–	–	$>-14.39\pm0.10$	–	–	–
ASASSN-14dq	-18.30 ± 0.50	–	-16.99 ± 0.01	-17.28 ± 0.01	-17.37 ± 0.01	-17.60 ± 0.03	8.72 ± 0.19
SN2014cw	–	–	–	-13.57 ± 0.04	-13.45 ± 0.01	-12.78 ± 0.08	6.97 ± 0.10
ASASSN-14kp	-16.87 ± 0.52	–	–	–	–	–	–
SN2015V	-18.50 ± 0.36	–	-17.45 ± 0.01	-17.76 ± 0.02	-17.67 ± 0.03	-18.07 ± 0.01	8.72 ± 0.19
SN2015W[a]	-18.62 ± 0.51	–	-18.27 ± 0.04	-18.54 ± 0.06	-18.55 ± 0.16	-18.33 ± 0.04	8.43 ± 0.34
SN2015aq	-16.51 ± 0.28	-14.09 ± 0.42	-16.57 ± 0.06	-17.08 ± 0.06	-17.11 ± 0.07	-17.03 ± 0.13	8.73 ± 0.05
SN2015bm	–	–	-14.36 ± 0.03	-14.81 ± 0.03	-15.03 ± 0.04	-15.11 ± 0.13	7.88 ± 0.08
SN2015bs	–	–	–	-12.20 ± 0.10	–	–	–
ASASSN-15kz	-18.06 ± 0.11	–	-17.54 ± 0.01	-17.72 ± 0.02	-17.82 ± 0.01	-17.40 ± 0.11	8.81 ± 0.10
ASASSN-15lx	-18.28 ± 0.20	–	–	–	–	–	–
ASASSN-15oz	–	–	–	$>-17.29\pm0.10$	–	–	–
ASASSN-15rp	–	–	–	$>-16.34\pm0.10$	–	–	–
SN2016B	-16.48 ± 0.03	-15.20 ± 0.01	-16.18 ± 0.01	-16.42 ± 0.01	-16.52 ± 0.01	-16.48 ± 0.01	8.26 ± 0.10
SN2016O	-15.58 ± 0.50	–	-14.17 ± 0.02	-14.73 ± 0.04	-14.53 ± 0.01	-14.49 ± 0.05	7.56 ± 0.10
SN2016X	-18.53 ± 0.12	-16.08 ± 0.15	-17.54 ± 0.01	-17.97 ± 0.10	-18.20 ± 0.01	-17.62 ± 0.01	8.71 ± 0.09
SN2016aqf	-17.66 ± 0.21	–	–	–	–	–	–
SN2016ase	-17.75 ± 0.20	–	-14.62 ± 0.09	-14.00 ± 0.19	-13.62 ± 0.11	–	8.01 ± 0.40
SN2016blz	-17.56 ± 0.41	-15.84 ± 0.02	-16.89 ± 0.01	-17.26 ± 0.01	-17.31 ± 0.01	-17.37 ± 0.02	8.70 ± 0.12
SN2016dbm	–	–	-17.93 ± 0.02	-18.17 ± 0.02	-18.45 ± 0.03	-18.43 ± 0.02	9.31 ± 0.25
SN2016dpd	–	–	-15.01 ± 0.03	-15.23 ± 0.07	-15.28 ± 0.02	-15.46 ± 0.11	7.99 ± 0.21
SN2016drl	–	–	–	$>-17.44\pm0.10$	–	–	–
SN2016egz	-16.36 ± 0.50	–	–	–	–	–	–
SN2016enk	-18.01 ± 0.38	-15.62 ± 0.08	-17.09 ± 0.01	-17.25 ± 0.01	-17.22 ± 0.14	-17.01 ± 0.74	8.58 ± 0.12
SN2016enp	–	-15.97 ± 0.09	-16.92 ± 0.03	-17.27 ± 0.01	-17.31 ± 0.02	-17.36 ± 0.08	8.69 ± 0.34
SN2016gsd	–	–	-16.79 ± 0.09	-16.87 ± 0.07	-17.38 ± 0.10	-16.94 ± 0.07	8.40 ± 0.39
SN2016hmq[a]	-18.39 ± 0.51	–	-18.54 ± 0.02	-19.05 ± 0.01	-19.28 ± 0.01	-19.43 ± 0.01	9.53 ± 0.03
SN2016hpt[a]	-18.81 ± 0.53	–	–	–	–	–	–
SN2017pn	–	–	-16.70 ± 0.02	-17.01 ± 0.03	-16.98 ± 0.02	-16.59 ± 0.05	8.38 ± 0.22
SN2017vp	–	-13.52 ± 0.57	-14.55 ± 0.12	-14.81 ± 0.14	-14.85 ± 0.16	-15.42 ± 0.34	7.56 ± 0.36
SN1986L	-21.34 ± 0.14	–	–	–	–	–	–
SN1990E	-19.27 ± 0.10	-16.77 ± 0.11	-18.25 ± 0.11	-18.99 ± 0.10	-19.43 ± 0.13	-19.74 ± 0.10	9.98 ± 0.36
SN1990K	-20.40 ± 0.12	–	-19.81 ± 0.10	-20.29 ± 0.13	-20.72 ± 0.10	-20.80 ± 0.13	10.21 ± 0.06
SN1991al	-21.18 ± 0.12	–	–	-20.23 ± 0.04	-20.32 ± 0.09	-20.20 ± 0.03	10.06 ± 0.19
SN1992af	-19.68 ± 0.21	–	–	–	–	–	–
SN1992am	-21.40 ± 0.33	-19.88 ± 0.02	-21.55 ± 0.10	-22.30 ± 0.05	-22.70 ± 0.22	-22.95 ± 0.02	11.17 ± 0.10
SN1992ba[b]	-17.99 ± 0.08	–	–	–	–	–	–
SN1993A	-18.90 ± 0.10	–	–	-20.02 ± 0.10	–	–	–
SN1993K	-20.85 ± 0.14	–	-19.78 ± 0.07	-19.91 ± 0.04	-21.06 ± 0.02	-20.82 ± 0.01	10.32 ± 0.17
SN1993S	-20.54 ± 0.29	–	–	–	–	–	–
SN1999br	-19.44 ± 0.09	-17.71 ± 0.09	-18.56 ± 0.23	-19.10 ± 0.01	-19.34 ± 0.11	-19.63 ± 0.21	9.71 ± 0.47
SN1999ca	-20.39 ± 0.04	–	–	–	–	–	–
SN1999cr	-20.39 ± 0.23	–	–	-18.64 ± 0.13	-19.15 ± 0.04	-19.09 ± 0.04	9.43 ± 0.09
SN1999eg	-20.73 ± 0.32	–	-18.58 ± 0.04	-19.03 ± 0.10	-19.31 ± 0.01	–	9.72 ± 0.41
SN1999em	-19.14 ± 0.15	–	–	–	-20.23 ± 0.10	–	–
SN2002ew	–	-18.03 ± 0.02	-19.12 ± 0.04	-19.41 ± 0.01	-19.61 ± 0.01	-19.76 ± 0.01	9.80 ± 0.13
SN2002fa	–	-19.15 ± 0.04	-20.26 ± 0.01	-20.69 ± 0.01	-20.96 ± 0.01	-21.15 ± 0.02	10.36 ± 0.25
SN2002gd	-19.82 ± 0.06	-17.57 ± 0.01	-18.96 ± 0.01	-19.62 ± 0.04	-19.91 ± 0.06	-20.21 ± 0.01	10.26 ± 0.03
SN2002gw	–	–	-20.40 ± 0.06	-20.53 ± 0.03	-20.67 ± 0.04	-20.67 ± 0.04	10.00 ± 0.08
SN2002hj	-17.98 ± 0.50	-17.51 ± 0.03	-18.56 ± 0.01	-18.92 ± 0.01	-19.12 ± 0.01	-19.22 ± 0.01	9.48 ± 0.18
SN2002hx	-20.99 ± 0.50	–	-19.16 ± 0.24	-21.17 ± 0.01	-21.49 ± 0.03	-21.46 ± 0.07	11.07 ± 0.14
SN2002ig[b]	–	-16.83 ± 0.09	-18.01 ± 0.02	-18.38 ± 0.02	-18.64 ± 0.02	-18.68 ± 0.06	9.36 ± 0.17
SN2003B	-21.42 ± 0.15	–	–	–	–	–	–
SN2003bl	–	-19.35 ± 0.01	-20.45 ± 0.01	-21.22 ± 0.14	-21.63 ± 0.10	-22.01 ± 0.10	11.02 ± 0.23
SN2003bn[b]	–	–	-17.31 ± 0.02	-17.58 ± 0.06	-18.09 ± 0.03	-18.16 ± 0.03	9.04 ± 0.07
SN2003ci	-22.14 ± 0.40	-20.12 ± 0.01	-21.37 ± 0.01	-22.00 ± 0.01	-22.36 ± 0.01	-22.59 ± 0.02	11.14 ± 0.34
SN2003cn	-20.61 ± 0.29	-19.16 ± 0.02	-20.40 ± 0.01	-20.91 ± 0.01	-21.19 ± 0.01	-21.34 ± 0.01	10.38 ± 0.20
SN2003cx[b]	–	–	-17.35 ± 0.01	-17.38 ± 0.03	-17.29 ± 0.03	-17.43 ± 0.12	8.37 ± 0.11
SN2003dq[b]	-17.52 ± 0.38	-17.15 ± 0.04	-17.89 ± 0.01	-17.95 ± 0.01	-18.02 ± 0.02	-17.92 ± 0.08	8.92 ± 0.15
SN2003E[b]	-17.99 ± 0.20	–	-17.64 ± 0.08	-18.25 ± 0.02	-18.20 ± 0.03	-18.35 ± 0.01	9.09 ± 0.02
SN2003ef	–	–	-20.39 ± 0.03	-20.98 ± 0.05	-21.10 ± 0.01	-21.46 ± 0.03	10.62 ± 0.29
SN2003eg	-22.26 ± 0.36	–	–	-21.43 ± 0.16	-21.35 ± 0.15	-22.78 ± 0.02	9.93 ± 0.04
SN2003ej	-20.87 ± 0.27	-18.73 ± 0.02	-20.00 ± 0.02	-20.49 ± 0.12	-20.75 ± 0.12	-20.89 ± 0.01	10.15 ± 0.16

Table 3 – *continued*

SN	Host M_B (mag)	Host M_u (mag)	Host M_g (mag)	Host M_r (mag)	Host M_i (mag)	Host M_z (mag)	Log($M_{\rm stellar}$) ($M_\odot$)
SN2003fb	− 20.89 ± 0.32	–	− 20.67 ± 0.05	− 21.01 ± 0.04	− 21.25 ± 0.01	− 21.34 ± 0.02	10.30 ± 0.08
SN2003gd	− 20.58 ± 0.26	–	− 18.05 ± 0.04	− 18.74 ± 0.02	− 19.24 ± 0.02	− 19.21 ± 0.06	9.80 ± 0.12
SN2003hd	− 21.73 ± 0.39	–	− 21.13 ± 0.01	− 21.70 ± 0.01	− 21.94 ± 0.01	− 22.09 ± 0.01	10.75 ± 0.36
SN2003hk	− 21.41 ± 0.52	− 20.01 ± 0.01	− 21.56 ± 0.01	− 22.32 ± 0.01	− 22.71 ± 0.01	− 23.01 ± 0.01	11.24 ± 0.38
SN2003hl	− 22.39 ± 0.54	− 18.85 ± 0.01	− 20.60 ± 0.01	− 21.42 ± 0.09	− 21.84 ± 0.07	− 22.14 ± 0.10	–
SN2003hn	− 21.06 ± 0.09	–	–	–	–	–	–
SN2003ho	− 19.85 ± 0.20	–	–	–	–	–	–
SN2003ib	− 20.78 ± 0.20	–	− 20.23 ± 0.01	− 20.83 ± 0.01	− 20.90 ± 0.03	− 21.18 ± 0.01	10.35 ± 0.14
SN2003ip	− 19.47 ± 0.32	− 17.35 ± 0.01	− 18.75 ± 0.01	− 19.38 ± 0.09	− 19.74 ± 0.01	− 19.96 ± 0.02	10.14 ± 0.06
SN2003iq	− 22.39 ± 0.54	− 18.85 ± 0.01	− 20.60 ± 0.01	− 21.42 ± 0.09	− 21.84 ± 0.07	− 22.14 ± 0.10	–
SN2003T	− 20.72 ± 0.70	− 19.28 ± 0.01	− 21.14 ± 0.01	− 21.99 ± 0.01	− 22.41 ± 0.01	− 22.69 ± 0.01	11.10 ± 0.14
SN2004dy	− 21.79 ± 0.27	− 20.03 ± 0.01	− 21.51 ± 0.01	− 22.25 ± 0.02	− 22.66 ± 0.02	− 22.86 ± 0.11	11.50 ± 0.13
SN2004ej	− 21.55 ± 0.19	–	–	–	–	–	–
SN2004er	− 20.35 ± 0.50	− 19.09 ± 0.01	− 20.09 ± 0.01	− 20.68 ± 0.02	− 20.88 ± 0.06	− 21.01 ± 0.14	10.66 ± 0.17
SN2004fb	− 20.88 ± 0.20	–	–	–	–	–	–
SN2004fc	− 19.51 ± 0.07	− 18.00 ± 0.01	− 19.26 ± 0.01	− 19.92 ± 0.10	− 20.22 ± 0.12	− 20.46 ± 0.10	10.45 ± 0.09
SN2004fx	–	–	− 18.78 ± 0.01	− 19.47 ± 0.03	− 19.84 ± 0.01	− 19.94 ± 0.02	10.13 ± 0.09
SN2005af	− 20.54 ± 0.20	–	–	–	–	–	–
SN2005an	− 18.62 ± 0.19	–	− 18.70 ± 0.01	− 18.72 ± 0.03	− 19.76 ± 0.01	− 19.90 ± 0.01	9.87 ± 0.05
SN2005dk	− 19.74 ± 0.20	–	–	–	–	–	–
SN2005dn	− 21.03 ± 0.11	–	–	–	–	–	–
SN2005dt	− 20.94 ± 0.23	–	− 20.15 ± 0.01	− 20.85 ± 0.05	− 21.25 ± 0.01	− 21.27 ± 0.03	10.52 ± 0.08
SN2005dw	− 21.12 ± 0.28	–	− 20.69 ± 0.01	− 21.25 ± 0.01	− 21.52 ± 0.02	− 21.69 ± 0.01	10.60 ± 0.07
SN2005dx	− 20.75 ± 0.43	–	− 22.40 ± 0.01	− 21.99 ± 0.10	− 20.64 ± 0.06	− 20.69 ± 0.02	10.99 ± 0.42
SN2005dz	− 19.85 ± 0.32	− 18.20 ± 0.01	− 19.83 ± 0.01	− 20.46 ± 0.01	− 20.72 ± 0.01	− 20.89 ± 0.01	10.35 ± 0.07
SN2005es	− 21.10 ± 0.41	− 19.66 ± 0.02	− 21.24 ± 0.02	− 21.97 ± 0.02	− 22.36 ± 0.01	− 22.69 ± 0.00	11.13 ± 0.22
SN2005J	− 20.41 ± 0.30	− 18.33 ± 0.01	− 19.97 ± 0.01	− 20.75 ± 0.01	− 21.11 ± 0.01	− 21.38 ± 0.01	10.47 ± 0.18
SN2005K	− 20.25 ± 0.49	− 18.85 ± 0.01	− 19.80 ± 0.01	− 20.14 ± 0.01	− 20.32 ± 0.01	− 20.52 ± 0.01	10.05 ± 0.23
SN2005me	− 21.41 ± 0.12	–	–	–	–	–	–
SN2005Z	− 20.52 ± 0.40	− 19.53 ± 0.01	− 20.95 ± 0.01	− 21.68 ± 0.01	− 22.11 ± 0.01	− 22.43 ± 0.01	11.05 ± 0.25
SN2006ai	− 19.22 ± 0.20	–	–	–	–	–	–
SN2006bc	− 20.89 ± 0.08	–	–	–	–	–	–
SN2006be	− 18.62 ± 0.32	− 16.52 ± 0.01	− 18.13 ± 0.01	− 18.93 ± 0.01	− 19.38 ± 0.01	− 19.85 ± 0.01	10.09 ± 0.20
SN2006bl	− 21.04 ± 0.33	− 19.65 ± 0.01	− 20.85 ± 0.01	− 21.35 ± 0.01	− 21.63 ± 0.01	− 21.82 ± 0.01	10.67 ± 0.44
SN2006it	− 21.10 ± 0.33	–	− 20.91 ± 0.16	− 21.74 ± 0.06	− 21.61 ± 0.12	− 22.11 ± 0.05	10.99 ± 0.39
SN2006iw	− 18.74 ± 0.50	− 16.89 ± 0.19	− 18.46 ± 0.01	− 18.97 ± 0.02	− 19.26 ± 0.02	− 19.51 ± 0.04	9.73 ± 0.21
SN2006ms	− 21.34 ± 0.09	–	–	–	–	–	–
SN2006qr	− 20.24 ± 0.50	–	− 19.55 ± 0.02	− 20.34 ± 0.01	− 20.60 ± 0.01	− 20.75 ± 0.01	10.18 ± 0.13
SN2006Y[b]	− 16.32 ± 0.15	–	–	–	–	–	–
SN2007aa	− 21.17 ± 0.19	− 17.88 ± 0.01	− 19.42 ± 0.01	− 20.19 ± 0.01	− 20.60 ± 0.01	− 20.94 ± 0.05	10.30 ± 0.06
SN2007ab	− 21.26 ± 1.25	–	− 20.64 ± 0.01	− 21.62 ± 0.06	− 22.06 ± 0.06	− 22.29 ± 0.07	11.52 ± 0.14
SN2007av	− 20.19 ± 0.28	− 17.00 ± 0.01	− 18.90 ± 0.01	− 19.75 ± 0.10	− 20.21 ± 0.10	− 20.63 ± 0.10	10.36 ± 0.16
SN2007hm	− 18.50 ± 0.50	− 17.05 ± 0.06	− 18.55 ± 0.01	− 18.97 ± 0.01	− 19.18 ± 0.01	− 19.34 ± 0.02	9.60 ± 0.16
SN2007il	− 20.87 ± 0.32	− 19.15 ± 0.01	− 20.42 ± 0.01	− 20.94 ± 0.01	− 21.18 ± 0.01	− 21.35 ± 0.01	10.50 ± 0.12
SN2007it	− 19.59 ± 0.16	–	–	–	–	–	–
SN2007oc	− 19.86 ± 0.27	–	–	–	− 21.22 ± 0.08	–	–
SN2007sq	− 22.22 ± 0.50	–	− 20.10 ± 0.01	− 21.17 ± 0.04	− 21.62 ± 0.02	− 21.94 ± 0.06	11.33 ± 0.14
SN2007W	− 20.91 ± 0.08	–	− 19.41 ± 0.03	− 19.790 ± 0.03	− 20.00 ± 0.03	− 19.92 ± 0.08	9.76 ± 0.04
SN2007X	− 20.45 ± 0.20	–	–	–	–	–	–
SN2007Z	− 22.84 ± 0.10	–	− 20.34 ± 0.10	− 21.83 ± 0.10	− 21.83 ± 0.10	− 22.03 ± 0.10	11.57 ± 0.20
SN2008ag	− 21.47 ± 0.11	–	–	–	–	–	–
SN2008aw	− 22.29 ± 0.07	–	− 20.46 ± 0.01	− 20.58 ± 0.14	− 20.57 ± 0.12	− 20.50 ± 0.12	9.68 ± 0.12
SN2008bh	− 20.93 ± 0.11	− 18.07 ± 0.01	− 20.15 ± 0.01	− 20.93 ± 0.01	− 21.46 ± 0.01	− 21.77 ± 0.01	11.25 ± 0.04
SN2008bk[b]	− 18.49 ± 0.15	–	–	–	–	–	–
SN2008bm	− 19.98 ± 0.71	− 18.64 ± 0.02	− 19.65 ± 0.02	− 20.00 ± 0.15	− 20.22 ± 0.13	− 20.32 ± 0.01	9.95 ± 0.42
SN2008bp	− 20.18 ± 0.09	–	− 19.28 ± 0.05	− 20.23 ± 0.02	− 20.53 ± 0.03	− 20.52 ± 0.02	10.08 ± 0.05
SN2008br	− 20.86 ± 1.17	–	–	–	–	–	–
SN2008bu	− 21.60 ± 0.50	–	–	–	–	–	–
SN2008F	− 20.33 ± 0.50	− 19.25 ± 0.01	− 20.89 ± 0.01	− 21.61 ± 0.01	− 22.00 ± 0.02	− 22.27 ± 0.02	10.92 ± 0.16
SN2008ga	–	–	− 18.06 ± 0.05	− 19.44 ± 0.02	− 19.94 ± 0.11	− 20.16 ± 0.02	10.72 ± 0.08
SN2008gi	− 20.01 ± 0.63	− 19.30 ± 0.01	− 20.37 ± 0.01	− 20.81 ± 0.01	− 21.03 ± 0.02	− 21.20 ± 0.01	10.42 ± 0.18
SN2008gr	− 20.55 ± 0.38	–	− 20.08 ± 0.02	− 20.45 ± 0.05	− 20.82 ± 0.01	− 20.85 ± 0.02	10.22 ± 0.08
SN2008H	− 21.54 ± 0.10	–	− 20.04 ± 0.10	− 20.63 ± 0.12	− 20.83 ± 0.12	− 20.85 ± 0.10	10.11 ± 0.09
SN2008ho	− 20.81 ± 0.09	–	− 20.40 ± 0.06	− 20.53 ± 0.03	− 20.68 ± 0.04	− 20.67 ± 0.04	10.00 ± 0.05

Table 3 – *continued*

SN	Host M_B (mag)	Host M_u (mag)	Host M_g (mag)	Host M_r (mag)	Host M_i (mag)	Host M_z (mag)	Log($M_{stellar}$) ($M_\odot$)
SN2008if	− 20.48 ± 0.44	–	− 20.65 ± 0.13	− 20.65 ± 0.16	− 20.57 ± 0.12	− 20.86 ± 0.05	9.66 ± 0.35
SN2008il	− 20.60 ± 1.03	–	–	–	–	–	–
SN2008in	− 20.36 ± 0.06	− 16.57 ± 0.01	− 18.10 ± 0.01	− 18.98 ± 0.01	− 19.44 ± 0.01	− 19.72 ± 0.01	10.60 ± 0.05
SN2008M	− 20.38 ± 0.20	–	–	–	–	–	–
SN2008W	− 20.60 ± 0.50	–	− 20.67 ± 0.01	− 20.30 ± 0.01	− 20.90 ± 0.03	− 21.02 ± 0.01	9.77 ± 0.11
SN2009aj	− 19.23 ± 0.10	–	–	–	–	–	–
SN2009ao	− 20.67 ± 0.39	− 18.14 ± 0.01	− 19.77 ± 0.01	− 20.52 ± 0.01	− 20.94 ± 0.01	− 21.31 ± 0.01	10.52 ± 0.26
SN2009au	− 20.08 ± 0.19	–	− 18.22 ± 0.02	− 19.17 ± 0.01	− 19.35 ± 0.06	− 19.55 ± 0.02	10.09 ± 0.11
SN2009bu	− 20.83 ± 0.23	–	–	–	–	–	–
SN2009bz	− 19.35 ± 0.34	− 17.69 ± 0.01	− 18.51 ± 0.01	− 18.89 ± 0.14	− 19.00 ± 0.01	− 19.05 ± 0.02	9.46 ± 0.12
SN2009N	− 20.28 ± 0.30	–	− 18.92 ± 0.04	− 19.37 ± 0.04	− 19.49 ± 0.06	− 19.23 ± 0.14	9.33 ± 0.09

[a]*Note*. SNe II from our sample included in the high-luminosity group.
[b]SNe II from A16 included in the low-luminosity group.

3 MEASUREMENTS

We now turn to the measurements that we make on the SN photometry and spectra, and the host galaxies.

3.1 SN measurements

We measure several photometric and spectroscopic parameters in our SN II sample. These spectral and photometric measurements were performed following the prescriptions presented in Anderson et al. (2014) and Gutiérrez et al. (2017a). From the photometry, we measure in the V band the magnitude at maximum light (M_{max}), the plateau decline rate (s_2), the optically thick duration phase (OPT_d) and the plateau duration (P_d). Here, we define P_d as in Anderson et al. (2014): the duration from the inflection point (t_{tran}) between the initial decline (s_1) and the plateau decline (s_2), until the end of the plateau (t_{end}). We measured OPT_d between the explosion (t_0) and the end of the plateau (t_{end}), while s_2 was measured by fitting a straight line during the plateau phase. Given that P_d is estimated over the interval (t_{tran}, t_{end}), the number of SNe with available estimates is significantly smaller compared to OPT_d or s_2. This is because a better photometric coverage is necessary to calculate the t_{tran} and the t_{end}, compared to s_2. Fig. 2 presents an example light curve indicating these parameters.

From the spectra, we measure the expansion velocities and the pEWs for seven lines: Hα, Hβ, Fe II λ5018, Fe II λ5169, Na I d, Ba II λ6142, and Sc II λ6247. We estimated the expansion velocities using the relativistic Doppler equation and the rest wavelength of each line. Further details are presented in Gutiérrez et al. (2017a). The pEWs were measured by tracing a straight line across the absorption feature to mimic the continuum flux, as shown in the lower panel of Fig. 2. Note that in this paper, Na I d refers to the Doppler-broadened Na ID line forming in the SN ejecta, and not the narrow line caused by any surrounding circumstellar material or interstellar material along the line of sight in the SN host. The spectral parameters are measured at (or interpolated to) 50 d from explosion (+50 d). We estimate the explosion epochs using the prescriptions described in Gutiérrez et al. (2017a), and the epochs are listed in Table 1 together with the technique employed to determine them. Details about the explosion epoch estimates for the literature events can be found in Gutiérrez et al. (2017a). The final spectroscopic and photometric properties are presented in Table 4.

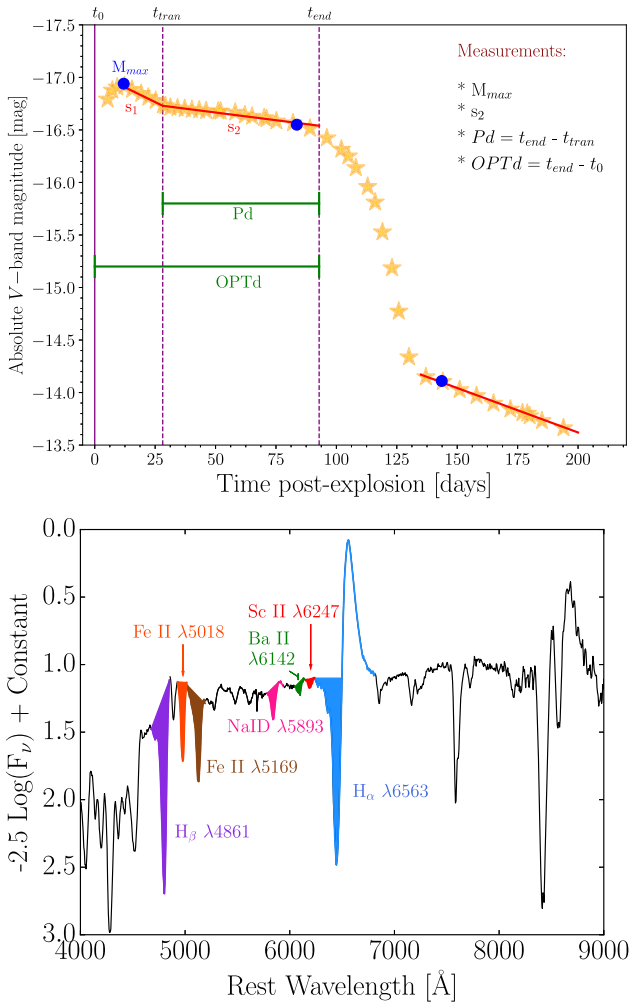

Figure 2. Definition of the measurements for our sample. The upper panel shows the light-curve parameters measured for each SN in the V band. The lower panel shows the absorption lines for which we measure pEWs, shown in the photospheric +41 d spectrum of SN 2016aqf.

3.2 Galaxy measurements

We characterize the global properties of the SN II hosts using the stellar mass ($M_{stellar}$). We use a custom galaxy SED fitting code,

Table 4. Photometric and spectroscopic (+50 d) measurements.

SN	$M_V^{\max}$ (mag)	s_2 (mag 100 d^{-1})	P_d (d)	OPT$_d$ (d)	pEW(Hα) (Å)	pEW(Hβ) (Å)	pEW(Fe II 5018) (Å)	pEW(Fe II 5169) (Å)	pEW(Na I D) (Å)	pEW(Ba II 6142) (Å)	pEW(Sc II 6247) (Å)	vel(Na I d) (km s^{-1})
SN2009lq	− 17.44 ± 0.10	0.27 ± 0.05	33.7 ± 2.1	75.8 ± 2.9	–	–	–	–	–	–	–	–
ASASSN-14dq	− 16.70 ± 0.10	1.10 ± 0.10	–	88.6 ± 0.7	–	–	–	–	–	–	–	–
SN2014cw	–	–	–	–	60.0 ± 3.6	62.0 ± 3.2	10.1 ± 1.5	19.1 ± 1.4	4.1 ± 1.1	0.0 ± 0.0	0.0 ± 0.0	3220 ± 663
ASASSN-14kp	–	–	–	–	–	45.5 ± 4.3	13.0 ± 1.5	27.0 ± 4.5	0.0 ± 0.0	0.0 ± 0.0	0.0 ± 0.0	–
SN2015V	− 15.74 ± 0.10	0.31 ± 0.01	68.6 ± 1.2	96.4 ± 1.1	80.0 ± 2.0	54.0 ± 3.0	20.2 ± 1.0	30.2 ± 2.0	11.0 ± 1.5	3.0 ± 0.9	2.8 ± 0.8	3780 ± 660
SN2015W	–	–	–	–	30.2 ± 4.1	73.0 ± 3.2	8.1 ± 1.5	41.0 ± 3.3	0.0 ± 0.0	0.0 ± 0.0	0.0 ± 0.0	–
SN2015aq	− 15.99 ± 0.10	0.86 ± 0.02	34.9 ± 1.4	90.5 ± 1.0	60.1 ± 2.2	64.0 ± 2.5	11.1 ± 1.1	29.3 ± 3.1	32.0 ± 2.2	–	–	5700 ± 600
SN2015bm	–	0.49 ± 0.01	–	–	24.1 ± 3.0	70.0 ± 3.2	13.5 ± 1.1	41.3 ± 3.4	29.0 ± 1.8	7.1 ± 1.6	–	4100 ± 650
SN2015bs	− 17.54 ± 0.05	0.33 ± 0.04	39.5 .1	78.5 ± 5.0	42.1 ± 4.8	76.1 ± 2.9	5.5 ± 1.3	12.2 ± 2.2	13.0 ± 2.1	0.0 ± 0.0	0.0 ± 0.0	4000 ± 760
ASASSN-15kz	− 17.08 ± 0.11	0.37 ± 0.01	45.2 ± 0.6	72.9 ± 0.6	35.2 ± 2.6	45.0 ± 4.0	14.0 ± 1.2	33.4 ± 3.3	9.1 ± 1.8	0.0 ± 0.0	0.0 ± 0.0	3100 ± 420
ASASSN-15lx	− 17.16 ± 0.10	0.50 ± 0.01	49.7 ± 0.8	98.5 ± 0.8	23.4 ± 3.3	42.0 ± 3.5	18.3 ± 1.6	35.0 ± 4.5	0.0 ± 0.0	–	0.0 ± 0.0	–
ASASSN-15oz	− 17.80 ± 0.10	0.68 ± 0.01	–	–	33.0 ± 3.8	75.0 ± 4.2	9.2 ± 1.1	47.2 ± 3.6	21.1 ± 2.5	–	9.0 ± 1.2	7800 ± 730
ASASSN-15rp	–	–	–	–	–	–	–	–	–	–	–	–
SN2016B	− 16.62 ± 0.10	0.34 ± 0.01	73.4 ± 0.1	113.7 ± 0.2	35.0 ± 2.1	55.0 ± 2.0	14.5 ± 1.3	38.1 ± 2.2	9.1 ± 1.5	2.5 ± 0.7	3.3 ± 0.9	4610 ± 500
SN2016O	–	–	–	–	35.3 ± 2.8	55.0 ± 2.5	19.1 ± 1.8	32.3 ± 3.5	9.2 ± 2.5	0.0 ± 0.0	0.0 ± 0.0	2700 ± 310
SN2016X	− 17.09 ± 0.10	0.52 ± 0.01	59.1 ± 0.2	86.7 ± 0.2	40.1 ± 2.9	52.1 ± 3.1	9.7 ± 1.3	36.1 ± 2.5	5.3 ± 1.5	0.0 ± 0.0	2.0 ± 1.1	5159 ± 560
SN2016aqf	− 15.43 ± 0.10	− 0.08 ± 0.08	43.5 ± 0.6	79.3 ± 0.6	58.2 ± 4.0	42.0 ± 2.6	20.5 ± 1.3	28.2 ± 1.9	12.0 ± 2.3	5.7 ± 1.0	5.5 ± 0.6	2300 ± 320
SN2016ase	− 17.47 ± 0.06	0.64 ± 0.02	34.0 ± 3.3	71.3 ± 4.0	35.4 ± 5.1	51.0 ± 2.5	26.0 ± 1.9	80.1 ± 3.6	34.1 ± 4.0	0.0 ± 0.0	0.0 ± 0.0	6534 ± 700
SN2016blz	− 18.07 ± 0.06	0.73 ± 0.01	48.8 ± 0.4	80.0 ± 4.2	–	38.2 ± 3.2	10.1 ± 1.9	18.0 ± 2.5	15.0 ± 3.4	–	–	7500 ± 730
SN2016dbm	− 19.71 ± 0.10	0.59 ± 0.01	–	–	–	13.0 ± 3.1	0.0 ± 0.0	0.0 ± 0.0	0.0 ± 0.0	0.0 ± 0.0	0.0 ± 0.0	–
SN2016dpd	− 18.57 ± 0.10	–	–	–	12.2 ± 4.0	46.0 ± 3.8	–	–	25.1 ± 3.1	–	–	7800 ± 820
SN2016drl	–	–	–	–	20.0 ± 4.3	33.0 ± 2.9	0.0 ± 0.0	0.0 ± 0.0	–	–	–	–
SN2016egz	− 18.36 ± 0.10	0.53 ± 0.01	35.7 ± 0.6	66.7 ± 0.5	11.3 ± 2.3	32.0 ± 2.1	5.1 ± 2.2	12.5 ± 2.1	–	0.0 ± 0.0	0.0 ± 0.0	–
SN2016enk	–	–	–	–	56.1 ± 3.2	68.0 ± 3.5	14.1 ± 1.0	30.1 ± 3.4	17.0 ± 4.0	0.0 ± 0.0	0.0 ± 0.0	4476 ± 520
SN2016enp	− 17.93 ± 0.10	–	–	–	6.1 ± 1.0	12.2 ± 2.6	7.0 ± 2.2	7.2 ± 1.5	0.0 ± 0.0	–	–	–
SN2016gsd	–	–	–	–	40.2 ± 3.3	37.0 ± 3.0	0.7 ± 0.5	11.2 ± 3.7	10.2 ± 2.3	1.5 ± 1.1	3.5 ± 1.3	6000 ± 560
SN2016hmq	–	–	–	–	28.1 ± 5.7	27.0 ± 3.2	10.5 ± 1.1	25.1 ± 3.6	18.1 ± 3.4	1.8 ± 0.5	5.0 ± 0.7	5000 ± 500
SN2016hpt	− 18.77 ± 0.10	–	–	–	13.0 ± 3.1	15.3 ± 2.9	–	–	35.0 ± 5.1	–	–	6500 ± 700
SN2017pn	− 17.00 ± 0.10	1.64 ± 0.13	–	–	27.8 ± 3.5	64.0 ± 2.6	7.7 ± 1.2	24.3 ± 2.1	8.1 ± 1.2	0.0 ± 0.0	0.0 ± 0.0	6000 ± 250
SN2017vp	–	–	–	–	37.2 ± 3.5	58.0 ± 4.5	12.0 ± 0.8	27.1 ± 3.8	–	–	–	–
SN1986L	− 18.19 ± 0.20	1.26 ± 0.03	59.6 ± 0.7	93.7 ± 6.7	32.8 ± 4.1	48.2 ± 3.6	14.7 ± 1.8	36.7 ± 3.8	29.2 ± 2.7	0.0 ± 0.0	0.0 ± 0.0	5512 ± 486
SN1990E	–	− 0.76 ± 0.12	–	–	–	–	–	–	–	–	–	–
SN1990K	–	2.39 ± 0.08	–	–	42.7 ± 3.8	71.9 ± 4.4	10.9 ± 0.7	38.8 ± 2.1	50.3 ± 2.5	6.4 ± 0.4	5.9 ± 0.9	6363 ± 391
SN1991al	− 17.51 ± 0.15	1.45 ± 0.04	–	–	62.1 ± 5.8	67.5 ± 5.2	13.0 ± 1.7	27.2 ± 3.8	20.4 ± 1.2	6.4 ± 0.9	4.1 ± 1.2	7835 ± 876
SN1992af	− 17.33 ± 0.12	0.58 ± 0.03	–	47.0 ± 6.7	–	–	–	–	–	–	–	–
SN1992am	− 18.06 ± 0.05	0.98 ± 0.02	–	–	–	–	–	–	–	–	–	–
SN1992ba	− 15.34 ± 0.80	0.72 ± 0.02	–	107.0 ± 8.5	61.9 ± 4.2	47.0 ± 3.9	20.2 ± 2.5	30.1 ± 3.9	34.2 ± 3.7	7.9 ± 1.1	7.1 ± 0.9	4325 ± 847
SN1993A	− 16.44 ± 0.07	0.51 ± 0.03	–	–	–	–	–	–	–	–	–	–
SN1993K	− 17.92 ± 0.23	2.36 ± 0.08	–	–	27.8 ± 3.8	42.8 ± 2.7	18.9 ± 3.8	28.7 ± 1.9	27.1 ± 1.9	3.8 ± 1	3.8 ± 1.1	5488 ± 520
SN1993S	− 17.52 ± 0.07	2.34 ± 0.04	–	–	–	–	–	–	–	–	–	6071 ± 620
SN1999br	− 13.77 ± 0.40	0.14 ± 0.02	–	–	56.0 ± 3.1	33.8 ± 4.8	25.2 ± 1.5	43.1 ± 3.1	20.7 ± 1.9	12.9 ± 1.6	14.2 ± 1.0	1519 ± 759
SN1999ca	− 17.48 ± 0.21	1.65 ± 0.06	40.5 ± 0.9	79.5 ± 7.6	48.3 ± 2.7	78.9 ± 3.9	17.6 ± 1.3	64.1 ± 2.9	33.7 ± 2.1	5.4 ± 0.4	11.6 ± 0.8	6825 ± 337
SN1999cr	− 16.90 ± 0.10	0.49 ± 0.08	43.5 ± 1.7	79.1 ± 7.6	31.7 ± 4.2	37.6 ± 4.1	12.4 ± 1.7	24.9 ± 1.8	9.3 ± 2.2	0.0 ± 0.0	0.0 ± 0.0	4504 ± 224
SN1999eg	− 16.86 ± 0.10	1.72 ± 0.06	–	–	–	–	–	–	–	–	–	–
SN1999em	− 16.76 ± 0.07	0.30 ± 0.02	67.1 ± 2.1	96.0 ± 5.8	75.8 ± 5.1	40.3 ± 5.6	23.8 ± 1.8	43.6 ± 2.5	30.6 ± 1.8	6.7 ± 1.0	7.5 ± 1.2	3722 ± 451
SN2002ew	− 17.42 ± 0.08	2.87 ± 0.25	–	–	–	–	–	–	–	–	–	–
SN2002fa	− 16.95 ± 0.04	1.56 ± 0.11	–	68.3 ± 7.6	45.4 ± 3.9	52.4 ± 7.2	15.5 ± 3.1	36.5 ± 2.4	42.4 ± 2.4	0.0 ± 0.0	0.0 ± 0.0	5741 ± 663
SN2002gd	− 15.43 ± 0.28	0.15 ± 0.04	–	–	21.7 ± 3.3	39.8 ± 3.3	24.9 ± 3.5	59.3 ± 4.2	27.1 ± 5.1	3.8 ± 0.6	11.0 ± 2.1	3406 ± 273
SN2002gw	− 15.76 ± 0.23	0.22 ± 0.03	–	88.3 ± 5.8	61.4 ± 4.6	58.4 ± 4.6	18.2 ± 2.1	31.3 ± 2.7	13.5 ± 1.3	3.1 ± 1.1	3.8 ± 1.5	3889 ± 304
SN2002hj	− 16.91 ± 0.10	1.57 ± 0.05	–	90.2 ± 7.6	70.1 ± 5.3	71.7 ± 5.5	16.5 ± 2.9	40.8 ± 3.2	18.6 ± 1.9	0.0 ± 0.0	0.0 ± 0.0	5239 ± 345
SN2002hx	− 17.00 ± 0.07	1.51 ± 0.03	–	68.0 ± 9.5	88.8 ± 6.1	73.8 ± 4.8	20.8 ± 2.2	35.5 ± 3.0	53.1 ± 4.1	8.6 ± 1.2	1.3 ± 2.1	5408 ± 477
SN2002ig	− 17.66 ± 0.03	2.20 ± 0.12	–	–	–	–	–	–	–	–	0.0 ± 0.0	–
SN2003B	− 15.36 ± 0.28	0.65 ± 0.03	–	86.2 ± 11.4	60.1 ± 5.3	53.0 ± 4.5	23.4 ± 2.5	38.1 ± 2.3	28.6 ± 2.2	3.9 ± 0.9	8.8 ± 1.5	4051 ± 228
SN2003bl	− 15.35 ± 0.14	0.35 ± 0.02	–	95.8 ± 4.2	58.0 ± 4.3	37.1 ± 2.1	26.5 ± 2.5	38.3 ± 1.8	19.3 ± 1.6	11.7 ± 1.4	9.1 ± 1.9	2712 ± 582
SN2003bn	− 16.80 ± 0.16	0.32 ± 0.03	63.0 ± 10.5	93.0 ± 4.2	77.7 ± 5.4	55.3 ± 6.5	17.3 ± 2.6	36.0 ± 1.1	16.1 ± 2.3	3.2 ± 1.0	2.5 ± 1.1	4077 ± 397
SN2003ci	− 16.83 ± 0.07	1.91 ± 0.04	–	92.5 ± 8.5	50.6 ± 2.5	64.6 ± 3.2	15.8 ± 0.8	46.2 ± 3.6	55.1 ± 1.8	7.7 ± 0.4	4.2 ± 0.2	5907 ± 292
SN2003cn	− 16.26 ± 0.11	1.34 ± 0.04	48.9 ± 4.0	69.8 ± 5.0	43.7 ± 2.9	52.9 ± 4.7	21.1 ± 3.4	35.1 ± 2.9	18.2 ± 1.7	7.4 ± 1.5	7.1 ± 1.2	3836 ± 695
SN2003cx	− 16.79 ± 0.06	0.61 ± 0.04	–	90.8 ± 5.8	–	–	–	–	–	–	–	5993 ± 610

Table 4 – *continued*

SN	M_V^{max} (mag)	s_2 (mag 100 d^{-1})	P_d (d)	OPT$_d$ (d)	pEW(Hα) (Å)	pEW(Hβ) (Å)	pEW(Fe II 5018) (Å)	pEW(Fe II 5169) (Å)	pEW(Na I D) (Å)	pEW(Ba II 6142) (Å)	pEW(Sc II 6247) (Å)	vel(Na I d) (km s^{-1})
SN2003dq	− 16.69 ± 0.06	2.12 ± 0.16	–	–	–	–	–	–	–	–	–	–
SN2003E	− 15.70 ± 0.15	− 0.1 ± 0.03	–	101.4 ± 7.6	–	–	–	–	–	–	–	–
SN2003ef	− 16.72 ± 0.14	0.78 ± 0.02	–	92.9 ± 9.5	91.4 ± 7.3	27.9 ± 4.2	20.4 ± 1.7	28.3 ± 3.4	24.2 ± 1	1.9 ± 0.9	9.6 ± 1.2	4316 ± 484
SN2003eg	− 17.81 ± 0.13	1.73 ± 0.13	–	–	9.4 ± 1.1	60.6 ± 3.4	14.4 ± 1.5	38.6 ± 1.1	58.4 ± 1.3	7.1 ± 1.1	6.5 ± 0.8	6993 ± 468
SN2003ej	− 17.66 ± 0.12	3.29 ± 0.04	–	69.0 ± 5.8	–	–	–	–	–	–	–	6244 ± 600
SN2003fb	− 15.56 ± 0.12	0.46 ± 0.06	–	88.3 ± 6.7	73.7 ± 6.3	55.1 ± 2.2	18.1 ± 0.8	40 ± 2.3	25.0 ± 1.6	9.0 ± 1.8	7.1 ± 1.2	4749 ± 668
SN2003gd	–	2.22 ± 0.05	–	–	–	–	–	–	–	–	–	–
SN2003hd	− 17.29 ± 0.06	0.93 ± 0.04	–	84.4 ± 5.8	78.1 ± 5.2	56.8 ± 4.4	16.1 ± 2.1	33.9 ± 2	15.4 ± 2.3	0.0 ± 0.0	0.0 ± 0.0	4725 ± 234
SN2003hk	− 17.02 ± 0.10	1.61 ± 0.06	59.0 ± 2.3	87.0 ± 5.0	32.6 ± 2.4	39.2 ± 3.7	17.6 ± 2.3	34.6 ± 2.6	44.3 ± 1.1	0.0 ± 0.0	0.0 ± 0.0	5767 ± 286
SN2003hl	− 15.91 ± 0.30	0.76 ± 0.01	–	108.9 ± 5.8	50.4 ± 3.1	32.6 ± 5.9	22.1 ± 2.9	39.5 ± 3.1	35.9 ± 2.5	5.6 ± 1.6	1.1 ± 1.2	4527 ± 318
SN2003hn	− 16.74 ± 0.10	2.52 ± 0.07	58.3 ± 1.6	90.1 ± 10.4	61.4 ± 4.0	60.0 ± 4.4	17.5 ± 1.5	39.1 ± 3.7	31.5 ± 2.6	4.3 ± 0.9	5.3 ± 0.8	4470 ± 339
SN2003ho	–	2.25 ± 0.11	–	–	68.4 ± 4.8	69.1 ± 4.6	16.9 ± 1.9	42.7 ± 3.2	36.1 ± 1.9	0.0 ± 0.0	0.0 ± 0.0	5010 ± 248
SN2003ib	− 17.10 ± 0.09	1.64 ± 0.03	–	–	–	–	–	–	–	–	–	–
SN2003ip	− 17.75 ± 0.13	2.03 ± 0.03	–	80.7 ± 5.0	60.9 ± 4.2	71.2 ± 6.8	9.3 ± 2.2	43 ± 3.7	33.2 ± 2.6	4.9 ± 0.6	5.9 ± 1.1	6501 ± 413
SN2003iq	− 16.69 ± 0.30	0.72 ± 0.01	–	84.9 ± 3.6	84.2 ± 5.6	46.2 ± 4.2	21.3 ± 1.8	37.7 ± 3.1	32.3 ± 2.9	3.4 ± 1.2	6.0 ± 1.0	5123 ± 360
SN2003T	− 16.54 ± 0.08	0.69 ± 0.02	–	90.6 ± 10.4	58.5 ± 6	27.6 ± 3.1	22.9 ± 1.9	38.2 ± 3.6	35.1 ± 2.5	18.7 ± 6.7	10.2 ± 1.2	3996 ± 292
SN2004dy	− 16.03 ± 0.07	0.83 ± 0.09	25.5 ± 5.2	–	–	–	–	–	–	–	–	–
SN2004ej	− 16.62 ± 0.21	1.04 ± 0.04	–	97.1 ± 8.5	57.1 ± 3.8	48.6 ± 4.7	20.7 ± 1.7	44.0 ± 4.3	37.2 ± 3.1	6.4 ± 1.6	5.9 ± 1.7	4005 ± 326
SN2004er	− 16.74 ± 0.16	0.52 ± 0.02	57.3 ± 1.7	120.1 ± 5.0	74.4 ± 5.7	59.2 ± 4.7	10.7 ± 2.3	34.3 ± 2.8	16.2 ± 2.3	0.4 ± 0.6	2.6 ± 0.7	5771 ± 506
SN2004fb	− 16.19 ± 0.11	1.26 ± 0.07	–	–	70.1 ± 7.2	59.1 ± 3.4	18.7 ± 2.1	46.9 ± 4.4	41.6 ± 2.8	10.8 ± 1.0	10.4 ± 1.2	4798 ± 340
SN2004fc	− 16.21 ± 0.31	0.50 ± 0.05	68.1 ± 2.7	106.1 ± 3.2	34.8 ± 6.2	16.2 ± 4.8	18.7 ± 2.8	28.2 ± 3.1	23.1 ± 2.3	5.0 ± 1.1	6.6 ± 1.8	4194 ± 541
SN2004fx	− 15.58 ± 0.24	0.25 ± 0.02	–	68.4 ± 5.0	70.6 ± 4.7	55.7 ± 3.3	18.6 ± 3.1	30.7 ± 2.0	11.3 ± 1.2	2.7 ± 1.2	4.8 ± 1.4	2884 ± 389
SN2005af	–	0.40 ± 0.05	–	107.0 ± 15.3	–	–	–	–	–	–	—	
SN2005an	− 17.07 ± 0.18	1.85 ± 0.05	36.0 ± 0.6	74.7 ± 5.0	51.9 ± 3.8	74.4 ± 5.7	15.4 ± 1.6	42.8 ± 2.9	18.4 ± 1.8	0.0 ± 0.0	10.5 ± 0.9	4738 ± 560
SN2005dk	− 17.52 ± 0.14	1.10 ± 0.07	39.0 ± 1.5	82.2 ± 6.7	49.0 ± 3.3	57.6 ± 3.5	13.4 ± 1.2	32.7 ± 3.2	32.1 ± 1.6	4.2 ± 0.9	4.6 ± 0.9	6317 ± 709
SN2005dn	− 17.01 ± 0.24	1.48 ± 0.04	45.8 ± 3.3	78.7 ± 6.7	66.6 ± 4.1	77.9 ± 4.5	3.9 ± 1.1	48.0 ± 3.1	30.7 ± 2.4	0.0 ± 0.0	0.0 ± 0.0	6518 ± 627
SN2005dt	− 16.39 ± 0.09	0.58 ± 0.06	–	113.0 ± 9.5	–	–	–	–	–	–	–	–
SN2005dw	− 16.49 ± 0.13	0.98 ± 0.07	56.1 ± 2.6	92.6 ± 9.5	–	–	–	–	–	–	–	–
SN2005dx	− 16.05 ± 0.08	1.26 ± 0.05	–	90.0 ± 7.6	–	–	–	–	–	–	–	–
SN2005dz	− 16.57 ± 0.12	0.36 ± 0.10	32.4 ± 2.8	81.9 ± 5.0	77.2 ± 3.4	50.4 ± 4.1	20.3 ± 2.3	34.4 ± 2.8	0.0 ± 0.0	0.0 ± 0.0	0.0 ± 0.0	7397 ± 735
SN2005es	− 16.98 ± 0.06	0.98 ± 0.05	–	–	–	–	–	–	–	–	–	–
SN2005J	− 17.28 ± 0.14	1.04 ± 0.02	53.0 ± 1.9	97.0 ± 7.6	77.2 ± 5.5	64.0 ± 2.5	15.9 ± 2.5	36.6 ± 2.4	23.2 ± 1.4	4.8 ± 1.7	3.9 ± 1.3	4994 ± 386
SN2005K	− 16.57 ± 0.08	1.45 ± 0.14	–	–	–	–	–	–	–	–	–	–
SN2005me	− 16.83 ± 0.10	1.55 ± 0.10	43.9 ± 1.5	80.6 ± 6.7	–	–	–	–	–	–	–	–
SN2005Z	− 17.17 ± 0.11	1.76 ± 0.01	–	78.9 ± 6.7	65.9 ± 3.4	56.8 ± 4.3	12.7 ± 1.6	36.1 ± 3.7	49.2 ± 2.9	0.0 ± 0.0	0.0 ± 0.0	7375 ± 560
SN2006ai	− 18.06 ± 0.14	2.05 ± 0.04	38.3 ± 0.5	63.3 ± 5.8	15.4 ± 2.6	38.5 ± 3.4	15.0 ± 2.1	36.8 ± 4.1	35.4 ± 2.1	0.0 ± 0.0	0.0 ± 0.0	6184 ± 434
SN2006bc	− 15.18 ± 0.26	− 0.67 ± 0.05	–	–	–	–	–	–	–	–	–	–
SN2006be	− 16.47 ± 0.29	0.63 ± 0.02	43.8 ± 1.3	76.2 ± 6.7	62.2 ± 3.3	68.1 ± 3.0	15.1 ± 0.7	26.0 ± 2.1	20.0 ± 1.2	5.3 ± 1.0	0.0 ± 0.0	4431 ± 668
SN2006bl	− 18.23 ± 0.07	2.41 ± 0.06	–	–	–	–	–	–	–	–	–	–
SN2006it	− 16.20 ± 0.15	1.14 ± 0.10	–	–	–	–	–	–	–	–	–	–
SN2006iw	− 16.89 ± 0.07	1.00 ± 0.03	–	–	40.6 ± 4.2	38.1 ± 3.3	10.0 ± 0.7	16.0 ± 1.6	12.1 ± 2	0.0 ± 0.0	0.0 ± 0.0	5074 ± 724
SN2006ms	− 16.18 ± 0.15	− 0.05 ± 0.45	–	–	–	–	–	–	–	–	–	–
SN2006qr	− 15.99 ± 0.14	1.40 ± 0.02	–	96.8 ± 7.6	69.7 ± 4.6	61.9 ± 5.3	22.1 ± 1.9	44.0 ± 4.2	33.6 ± 2.4	8.8 ± 1.9	12.6 ± 1.2	4844 ± 554
SN2006Y	− 17.97 ± 0.06	2.11 ± 0.18	24.7 ± 0.6	47.5 ± 5.0	10.4 ± 2.9	25.5 ± 2.8	6.7 ± 1.8	16.3 ± 3.1	15.8 ± 1	0.0 ± 0.0	0.0 ± 0.0	7004 ± 613
SN2007aa	− 16.32 ± 0.27	− 0.05 ± 0.02	–	–	74.5 ± 6.5	52.5 ± 5.8	20.7 ± 1.8	35.1 ± 2.5	31.8 ± 2.9	1.1 ± 0.9	5.7 ± 1.6	3864 ± 321
SN2007ab	− 16.98 ± 0.09	3.18 ± 0.06	–	71.7 ± 10.4	72.4 ± 5.1	84.6 ± 5.4	17.5 ± 3.6	77.2 ± 3.4	32.9 ± 2	8.0 ± 1.1	12.0 ± 2.3	7285 ± 404
SN2007av	− 16.27 ± 0.22	0.92 ± 0.01	–	–	97 ± 6.6	46.4 ± 3.3	21.8 ± 1.4	43.9 ± 2.5	29.4 ± 3.2	7.6 ± 1.9	8.3 ± 1.5	3957 ± 605
SN2007hm	− 16.47 ± 0.09	1.52 ± 0.04	–	–	44.1 ± 4.3	56.2 ± 5.9	16.6 ± 3.3	29.1 ± 3.3	22.3 ± 2.2	0.0 ± 0.0	0.0 ± 0.0	5278 ± 262
SN2007il	− 16.78 ± 0.11	0.12 ± 0.04	68.7 ± 2.4	103.4 ± 5.0	63.9 ± 5.4	66.4 ± 4.2	13.4 ± 2.5	28.2 ± 6.3	15.6 ± 1.1	0.0 ± 0.0	0.0 ± 0.0	4798 ± 769
SN2007it	− 17.55 ± 0.50	1.33 ± 0.14	–	–	–	–	–	–	–	–	–	–
SN2007oc	− 16.68 ± 0.15	1.78 ± 0.01	42.8 ± 0.6	71.6 ± 5.8	35.5 ± 2.8	70.1 ± 6.9	8.0 ± 1.9	46.5 ± 4.6	43.6 ± 1.8	3.5 ± 1.5	2.9 ± 1.0	5019 ± 450
SN2007sq	− 15.33 ± 0.13	1.29 ± 0.08	44.7 ± 2.4	87.6 ± 5.0	37.5 ± 4.2	48.3 ± 4	6.8 ± 1.9	31.8 ± 3.5	22.4 ± 0.9	0.0 ± 0.0	0.0 ± 0.0	5662 ± 280
SN2007W	− 15.80 ± 0.20	0.00 ± 0.04	56.7 ± 2.6	83.6 ± 7.6	67.2 ± 3.6	38.1 ± 5.9	21.7 ± 2.6	36.5 ± 2.8	13.5 ± 2.2	4.6 ± 1.3	4.1 ± 1.3	2618 ± 186
SN2007X	− 17.84 ± 0.21	1.37 ± 0.03	53.9 ± 1.0	98.1 ± 5.8	45.2 ± 2.8	77.1 ± 4.7	13.9 ± 2.9	49.4 ± 2.1	22.9 ± 1.2	5.6 ± 0.9	9.1 ± 1.4	6170 ± 708
SN2007Z	–	–	–	–	–	–	–	–	–	–	–	–

Table 4 – *continued*

SN	M_V^{max} (mag)	s_2 (mag 100 d^{-1})	P_d (d)	OPT$_d$ (d)	pEW(Hα) (Å)	pEW(Hβ) (Å)	pEW(Fe II 5018) (Å)	pEW(Fe II 5169) (Å)	pEW(Na I D) (Å)	pEW(Ba II 6142) (Å)	pEW(Sc II 6247) (Å)	vel(Na I d) (km s^{-1})
SN2008ag	− 16.96 ± 0.15	0.12 ± 0.01	–	105.3 ± 6.7	60.6 ± 5.2	39.3 ± 3.2	22.3 ± 1.7	38.9 ± 2.6	38.4 ± 2.1	3.3 ± 1.8	5.5 ± 1.2	4215 ± 426
SN2008aw	− 17.71 ± 0.19	2.10 ± 0.05	37.9 ± 0.9	75.82 ± 10.4	17.8 ± 2.3	47.1 ± 4.6	12.4 ± 1.4	37.8 ± 1.4	38.8 ± 2.9	3.6 ± 1.6	3.6 ± 1.3	6436 ± 478
SN2008bh	− 16.06 ± 0.14	1.20 ± 0.04	–	–	55.8 ± 4.2	54.4 ± 5.6	16.2 ± 2.0	36.2 ± 1.1	16.7 ± 1.9	5.2 ± 0.9	5.2 ± 0.8	4683 ± 378
SN2008bk	− 14.86 ± 0.05	0.26 ± 0.01	–	107.2 ± 6.7	57.5 ± 4.8	31.9 ± 3.9	24.6 ± 2.1	43.7 ± 3.5	20.1 ± 1.7	11.8 ± 1.2	10.5 ± 1.1	2019 ± 171
SN2008bm	− 18.12 ± 0.07	2.50 ± 0.03	–	87.0 ± 26.2	4.6 ± 0.2	19.2 ± 1.3	11.6 ± 0.6	19.8 ± 2.1	3.4 ± 0.6	0.0 ± 0.0	0.0 ± 0.0	1762 ± 88
SN2008bp	− 14.00 ± 0.21	2.79 ± 0.13	–	58.6 ± 9.5	–	–	–	–	–	–	–	–
SN2008br	− 15.30 ± 0.20	0.38 ± 0.04	–	–	15.8 ± 3.0	22.3 ± 3.2	7.2 ± 1.1	9.7 ± 2.8	12.4 ± 0.7	9.4 ± 1.1	6.7 ± 2.5	1922 ± 96
SN2008bu	− 17.14 ± 0.10	2.37 ± 0.18	–	44.7 ± 7.6	–	–	–	–	–	–	–	–
SN2008F	− 15.67 ± 0.12	0.48 ± 0.10	–	–	–	–	–	–	–	–	–	–
SN2008ga	− 16.45 ± 0.14	1.10 ± 0.07	–	73.1 ± 5.0	85 ± 5.7	60.0 ± 2.3	17.0 ± 1.5	35.1 ± 2.1	55.0 ± 2.1	0.0 ± 0.0	0.0 ± 0.0	4785 ± 663
SN2008gi	− 17.31 ± 0.09	2.63 ± 0.11	–	–	–	–	–	–	–	–	–	–
SN2008gr	− 17.95 ± 0.10	1.61 ± 0.03	–	–	35.5 ± 3.5	56.6 ± 3.6	7.3 ± 0.9	34.1 ± 2.6	30.9 ± 2.5	0.0 ± 0.0	0.0 ± 0.0	7487 ± 708
SN2008H	–	–	–	–	63.3 ± 5.1	33.0 ± 3.1	22.2 ± 1.7	51.0 ± 3.2	54.1 ± 3.1	15.0 ± 2.2	14.0 ± 1.8	4669 ± 760
SN2008ho	− 15.11 ± 0.23	0.32 ± 0.07	–	–	–	–	–	–	–	–	–	–
SN2008if	− 17.94 ± 0.17	1.99 ± 0.02	51.0 ± 0.3	75.8 ± 5.8	26.1 ± 2.3	61.8 ± 3.7	9.3 ± 1.3	30.2 ± 3.3	48.3 ± 3.2	1.2 ± 0.5	3.7 ± 0.9	7404 ± 633
SN2008il	− 16.61 ± 0.11	0.71 ± 0.05	–	–	–	–	–	–	–	–	–	–
SN2008in	− 15.40 ± 0.47	0.91 ± 0.01	–	89.6 ± 6.7	54.8 ± 7.3	36.6 ± 3.1	26.9 ± 1.9	42.9 ± 2.7	38.8 ± 2.3	6.4 ± 1.4	8.3 ± 1.8	2917 ± 321
SN2008M	− 16.75 ± 0.28	0.94 ± 0.02	58.3 ± 0.3	75.3 ± 9.5	54.0 ± 5.5	72.9 ± 3.8	20.2 ± 3.4	34.0 ± 1.9	30.3 ± 2.8	2.5 ± 0.9	1.6 ± 1.1	4793 ± 1056
SN2008W	− 16.60 ± 0.11	1.10 ± 0.04	–	85.8 ± 6.7	46.7 ± 4.2	60.4 ± 3.4	16.4 ± 2.9	36.9 ± 2.8	45.9 ± 1.7	3.5 ± 1.4	4.6 ± 1.7	5244 ± 470
SN2009aj	− 18.07 ± 0.20	–	–	–	8.1 ± 1.6	13 ± 2.2	8.5 ± 0.9	13.9 ± 3.1	1.7 ± 0.6	0.0 ± 0.0	0.0 ± 0.0	3026 ± 240
SN2009ao	− 15.79 ± 0.20	− 0.01 ± 0.12	–	41.7 ± 5.0	40.2 ± 3.1	54.5 ± 3.4	18.5 ± 1.4	41.8 ± 2.7	24.2 ± 1.6	0.0 ± 0.0	9.1 ± 1.8	4687 ± 335
SN2009au	− 16.34 ± 0.21	3.03 ± 0.02	–	–	5.9 ± 1.4	12.8 ± 2.7	11.9 ± 1.7	17.2 ± 2.5	7.9 ± 0.8	3.3 ± 0.6	5.6 ± 1.3	1949 ± 118
SN2009bu	− 16.05 ± 0.19	0.13 ± 0.04	–	–	84.6 ± 5.3	55.9 ± 3.1	14.2 ± 1.9	26.4 ± 1.8	15.1 ± 1.5	0.0 ± 0.0	0.0 ± 0.0	4378 ± 308
SN2009bz	− 16.46 ± 0.19	0.36 ± 0.03	–	–	–	–	–	–	–	–	–	–
SN2009N	− 15.25 ± 0.40	0.22 ± 0.01	66.7 ± 0.5	89.8 ± 5.8	75.7 ± 3.1	39.1 ± 3.9	25.4 ± 1.6	34.4 ± 2.1	24.5 ± 1.2	10.3 ± 1.6	9.6 ± 1.1	2705 ± 186

Table 5. Sample details.

	SNe II in LLH	SNe II in HLH	Total
Full sample	**35**	**103**	**138**
New SNe	27	3	30
SNe from A16	8	100	108
SNe with light curve in V band	29	103	132
SNe with spectra around 50 d	28	72	100
SNe with $M_B^{\rm host}$ data	19	95	114
SNe with $M_r^{\rm host}$ data	28	74	102

following Sullivan et al. (2010). The code is similar to Z-PEG (Le Borgne & Rocca-Volmerange 2002), with an expanded set of templates based on the galaxy spectral synthesis code PÉGASE.2 (Fioc & Rocca-Volmerange 1997). Specifically, the code uses a set of 15 exponentially declining star formation histories (SFHs), each with 125 age steps, assuming a Salpeter (1955) initial mass function (IMF). The internal PÉGASE.2 dust prescription is not included in the templates, but instead extinction is included as a foreground dust screen with $E(B-V)=0$ to 0.3 mag in steps 0.05 mag. The code determines the best-fitting SED model by minimization of the χ^2 using data in the *uBgriz* filters. The redshift in the fit is fixed to the value of the SN redshift.

The $M_{\rm stellar}$ of the host galaxy is calculated by integrating the star formation history of the best-fitting SED model, subtracting the mass of the stars that have died. The $M_{\rm stellar}$ uncertainties are calculated by performing a Monte Carlo simulation on the observed galaxy fluxes according to the uncertainties retrieved from SDSS. Table 3 gives the final information on the host galaxies.

4 RESULTS

In this section, we compare the SNe II in low-luminosity galaxies with those located in high-luminosity hosts, searching for significant differences in SN properties between the two samples. All spectral comparisons are performed at +50 d.

4.1 SNe II in fainter galaxies versus SNe II in brighter galaxies

We split our full sample into two: 35 SNe II located within 'faint' host galaxies, defined as $M_r \gtrsim -18.5$ mag (or $M_B \gtrsim -18.5$ mag, where no r-band data is available), and 103 SNe II in 'bright' host galaxies, defined as $M_r < -18.5$ mag (or $M_B < -18.5$ mag). This absolute magnitude limit is around the brightness of the well-studied LMC. This was chosen as the separation limit because very few SN II were observed in the sample used by D14 with inferred metallicities below that of the LMC, hence we investigate whether SNe II dimmer than this limit are distinct from those in brighter hosts. Details about the characteristics of low- and high-luminosity groups are presented in Table 5.

4.1.1 SN photometric properties

The photometric properties for our sample are shown in Fig. 3. Our SNe II cover a wide range of observed properties, with no clear distinction between those in low- and high-luminosity hosts for $M_V^{\rm max}$, $P_{\rm d}$, and $\rm OPT_d$. However, the mean s_2 in high-luminosity hosts is 1.19 ± 0.09 mag $100\,{\rm d}^{-1}$, compared to 0.72 ± 0.13 mag $100\,{\rm d}^{-1}$ in low-luminosity hosts. This suggests that SNe II in lower luminosity hosts have a shallower decline during the recombination phase.

Fig. 3 also shows the cumulative distributions for the three photometric parameters. Throughout this paper, we compare such cumulative distributions of SN parameters for events in low- and high-luminosity host galaxies. For this, we use the Kolmogorov–Smirnov (KS) test, a non-parametric test that compares the cumulative distributions of two data sets under the null hypothesis that both groups are sampled from populations with identical distributions. We reject this null hypothesis when $\rho_{\rm KS} < 0.01$. In this case (Fig. 3), the KS test shows that we can reject the null hypothesis that both s_2 samples (in high- and low-luminosity hosts) are drawn from parent populations with the same distributions. The mean values and corresponding KS test results are in Table 6.

4.1.2 SN spectral properties

We see no significant differences in the velocities of SNe II located in low- and high-luminosity hosts. An example is shown in Fig. 4, showing the expansion velocity for Na I d. Only small differences of $\sim$50 km s^{-1} are observed. The figure also shows that both groups have a similar velocity distribution, with a large range of velocity values. Similar behaviour is observed for the rest of the SN velocities, suggesting that the SN explosion energy is not significantly affected by metallicity. A complete set of measurements can be found in Table 6.

Fig. 5 shows the pEW distributions for Fe IIλ5018, Hα absorption, Na I d and Sc II λ6247 for the high- and low-luminosity host samples. In general, the pEWs for SNe II in low-luminosity hosts are shifted to smaller values. The result obtained for pEW(Fe II 5018) is consistent with the prediction of D14, who found that the strength of the metal lines increases with increasing progenitor metallicity; SNe II with metal-poor progenitors should have weaker iron lines. Using host luminosity as a proxy for host metallicity confirms this prediction observationally. The Na ID line shows a similar behaviour, but, for the Hα line, the opposite to that predicted by D14 is observed, where higher metallicity models show weaker Hα absorption. The comparison of the pEWs of Hβ, Fe IIλ5169, and Ba II λ6142 for SNe II for low- and high-luminosity hosts showed similar results to those in Fig. 5.

The cumulative distributions for the pEW differences are also shown in Fig. 5. KS tests reject the null hypothesis that the distributions of the pEWs in low- and high-luminosity hosts are drawn from populations with the same distribution for all four lines. The differences are most significant for Na I d and Sc II λ6247, with $\rho_{\rm KS}$ less than $\sim$0.0001 and $\sim$0.002, respectively. The mean pEWs obtained for all seven lines in the low- and high-luminosity hosts, and the corresponding KS test values, are presented in Table 6.

Fig. 6 shows the temporal evolution of pEW(Fe II 5018), compared to the synthetic spectra at four different metallicities (see D14). pEW(Fe II 5018) for SNe II in high-luminosity hosts lies around the model with solar metallicity ($Z_\odot$), while SNe II in low-luminosity hosts are closer to the 0.4 $Z_\odot$ model. This is again consistent with the low-luminosity host group sampling SN II progenitors of lower metallicity than the high-luminosity group.

Fig. 6 also shows that the pEW(Fe II 5018) for SNe II in high-luminosity hosts evolves faster at early phases. To quantify this, we measure the rate of change of the pEW (ΔpEW) over the intervals [+10, +35], [+ 35, +55], and [+ 55, 90] d. For low-luminosity hosts,

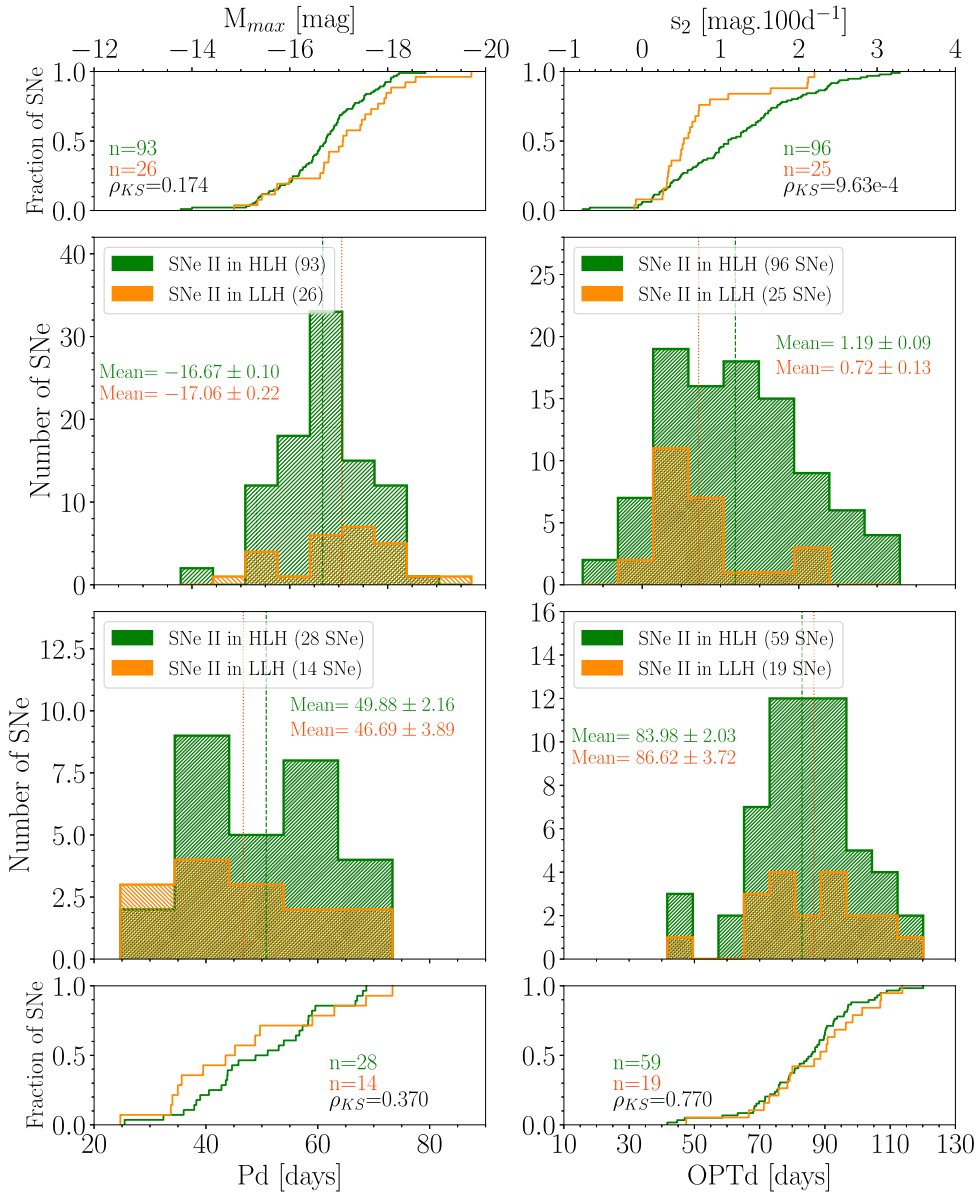

Figure 3. The distribution of the SN II light curve properties $M_V^{\max}$ (top left), s_2 (top right), $P_{\rm d}$ (bottom left), and OPT$_{\rm d}$ (bottom right) in low-luminosity hosts (LLH; orange) and high-luminosity hosts (HLH; green). The upper row shows the histograms of each property, and the lower row shows the cumulative distributions. The vertical lines indicate the mean for each distribution. In the lower panels, the number of events (n) and the $\rho_{\rm KS}$ are given.

ΔpEW is 0.24 ± 0.04, 0.29 ± 0.07, and 0.20 ± 0.08 Å d^{-1}, while in high-luminosity hosts the values are 0.39 ± 0.03, 0.25 ± 0.05, and 0.16 ± 0.04 Å d^{-1}: at early phases, the pEW evolves ∼40 per cent faster in SNe II in high-luminosity hosts than in low-luminosity host, but becomes consistent at later phases.

In the models, for the 0.4 Z$_\odot$ model, the ΔpEW is 0.42 ± 0.05, 0.13 ± 0.05, and $0.30 \pm 0.0.06$ Å d^{-1}, while for the Z$_\odot$ model they are 0.53 ± 0.03, 0.27 ± 0.04, and 0.29 ± 0.05 Å d^{-1}. In the first two intervals, the pEW at Z$_\odot$ evolves faster than the pEW at 0.4 Z$_\odot$, but in the last interval, they are almost the same. Comparing the models with the observed SNe, the Z$_\odot$ model displays a faster evolution at all epochs in comparison with observed SNe II, however, for the model at lower metallicity, the evolution is faster only in the first interval.

4.2 Correlations between SN II properties and host galaxy parameters

We next investigate any dependence of SN II diversity on environmental parameters, specifically the absolute magnitudes and stellar masses of the host galaxies. In particular, we examine pEW(Fe II 5018) and pEW(Na I D) for our SNe II in the context of the SN host galaxies. We use pEW(Fe II 5018) as the models show that it is mainly affected by the metallicity of the progenitor, and we use pEW(Na I D) due to the significance of the relations seen in Fig. 5 and presented in Table 6.

Fig. 7 shows the relation between the host galaxy absolute magnitudes in different filters (*riz*), and pEW(Fe II 5018) and pEW(Na I D). In general, SNe II in lower luminosity hosts have smaller pEW values. Using the Pearson correlation test, we

Table 6. Mean values and KS test results.

Parameter	Mean values in the high-luminosity host group	Mean values in the low-luminosity host group	ρ_{KS}
M_V^{max}	-16.67 ± 0.10 mag (93)	-17.06 ± 0.22 mag (26)	0.174
s_2	1.19 ± 0.09 mag 100 d^{-1} (96)	0.72 ± 0.13 mag 100 d^{-1} (25)	**9.63×10^{-4}**
P_d	49.88 ± 2.16 d (28)	46.69 ± 3.89 d (14)	0.369
OPT_d	83.98 ± 2.03 d (59)	86.62 ± 3.72 d (19)	0.769
vel(Hα)	7040 ± 195 km s^{-1} (75)	7625 ± 410 km s^{-1} (26)	0.153
vel(Hβ)	5640 ± 175 km s^{-1} (75)	5960 ± 280 km s^{-1} (28)	0.728
vel(Fe II 5018)	3965 ± 130 km s^{-1} (73)	3695 ± 235 km s^{-1} (25)	0.281
vel(Fe II 5169)	3880 ± 115 km s^{-1} (73)	3755 ± 240 km s^{-1} (25)	0.184
vel(Na I d)	4815 ± 170 km s^{-1} (70)	4860 ± 390 km s^{-1} (21)	0.587
vel(Ba II 6142)	3685 ± 180 km s^{-1} (50)	3630 ± 865 km s^{-1} (6)	0.746
vel(Sc II 6247)	3530 ± 135 km s^{-1} (50)	4020 ± 650 km s^{-1} (8)	0.716
pEW(Hα)	52.37 ± 2.65 Å (72)	39.12 ± 4.10 Å (25)	**7.7×10^{-3}**
pEW(Hβ)	51.26 ± 2.04 Å (72)	48.19 ± 3.15 Å (28)	0.444
pEW(Fe II 5018)	16.52 ± 0.63 Å (71)	12.21 ± 1.36 Å (27)	**7.55×10^{-3}**
pEW(Fe II 5169)	36.60 ± 1.24 Å (71)	27.51 ± 3.14 Å (27)	**1.18×10^{-3}**
pEW(Na I D)	28.14 ± 1.63 Å (72)	14.02 ± 2.11 Å (25)	**1.01×10^{-4}**
pEW(Ba II 6142)	4.04 ± 0.49 Å (71)	2.13 ± 0.76 Å (20)	0.024
pEW(Sc II 6247)	4.65 ± 0.50 Å (71)	2.09 ± 0.68 Å (22)	**1.99×10^{-3}**

Note. The number of events used for each measurement are given in parenthesis. ρ_{KS} lower than 0.01 are presented in bold.

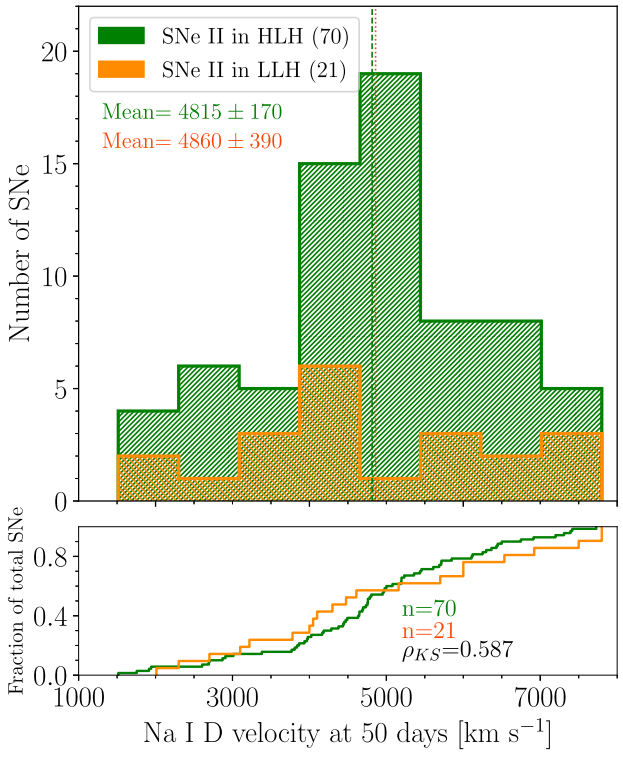

Figure 4. The distribution of Na ID velocity at 50 d from explosion (upper panel) and the cumulative distribution (lower panel). SNe II in low-luminosity hosts are in orange, and those in high-luminosity hosts in green. The vertical lines indicate the mean for each distribution. In the cumulative distribution panel, the number of SNe and the ρ_{KS} are shown.

find weak anti-correlations for pEW(Fe II 5018) of $\rho = -0.34$, -0.23 and -0.37, and moderate anticorrelations for pEW(Na I D): $\rho = -0.46$, -0.44, and -0.52. The strongest correlations are observed in the z-band.

Fig. 8 shows the relation between pEW(Fe II 5018) and pEW(Na I D) with $M_{stellar}$. The correlation between $M_{stellar}$ and pEW(Fe II 5018) is weak ($\rho = 0.31$), while the correlation between $M_{stellar}$ and pEW(Na I D) is moderate ($\rho = 0.44$). SNe II with a smaller pEW(Na I D) preferentially occur in low $M_{stellar}$ galaxies. By contrast, SNe II with a higher pEW(Na I D) are found in galaxies with a larger $M_{stellar}$. To test the significance of the correlation between pEW(Na I D) and $M_{stellar}$, we use a Monte Carlo resampling with 10^5 random draws. Varying both parameters according to their 1σ uncertainties and a Gaussian distribution, we estimate the Pearson coefficient (ρ) for each iteration. The median of ρ is 0.47, which is consistent with our findings.

Using a KS test, we probe the differences between SNe II in low/high $M_{stellar}$. The KS test rejects the null hypothesis that the distributions of the pEW(Fe II 5018) in low and high $M_{stellar}$ are drawn from populations with the same distribution. The differences are more significant for pEW(Na I D). To test this result and using a Monte Carlo resampling (varying the pEW values using 1σ uncertainties according to a Gaussian distribution), we find a statistically significant difference between the $M_{stellar}$ when comparing the pEW(Na I D).

Given that our comparison models produce SN II light curves and spectra that are qualitatively similar to observed SN IIP (slow decliners), we may expect stronger correlations when restricting our sample to slow-declining events. Surprisingly, we find the opposite: correlations decrease in strength when removing the fastest decliners.

5 DISCUSSION

Using a sample of SNe II and their host galaxies, we have examined various relationships between SN II properties and their host galaxies to probe the role of metallicity in SN II evolution and diversity. Following D14, we tested the influence of metallicity on the strength of the SN metal lines. Our main result is that SNe II

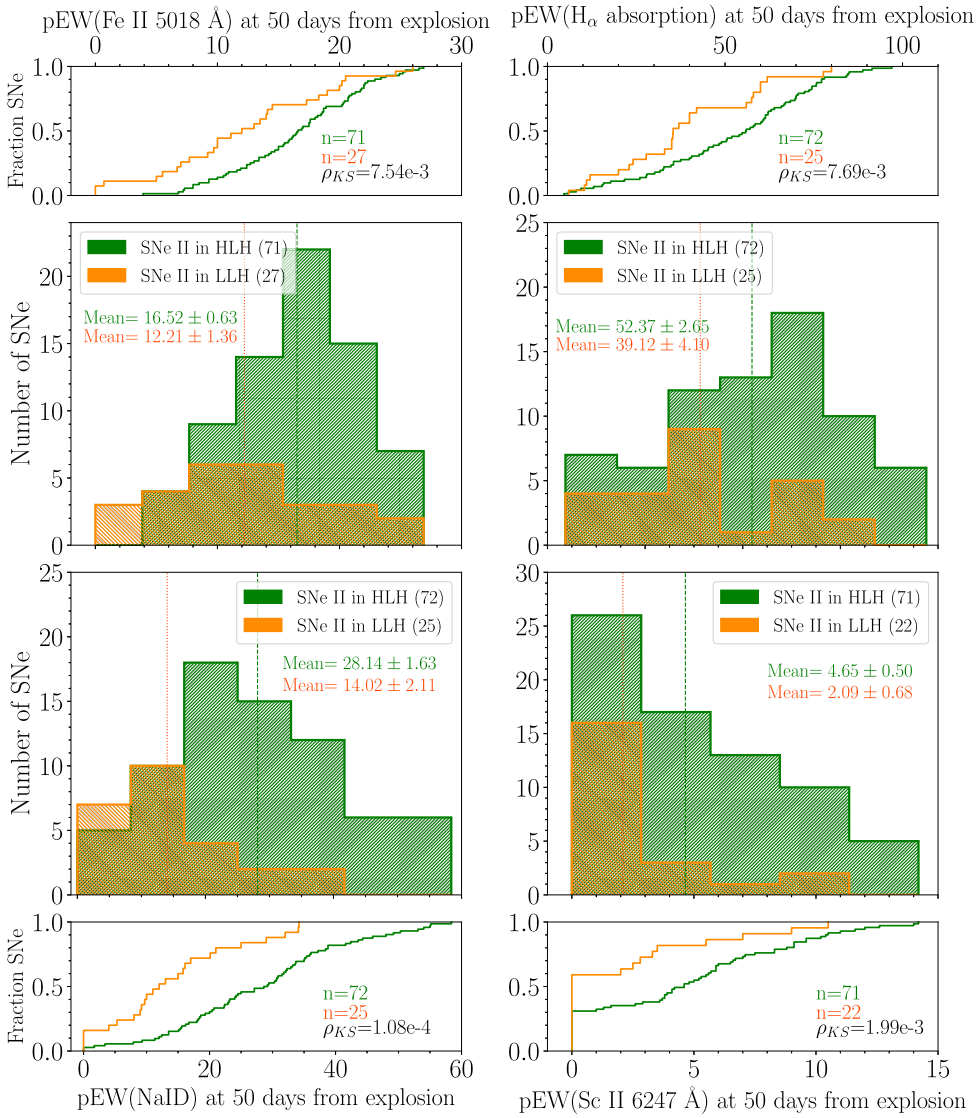

Figure 5. Distribution of the pEW absorption measurements for SNe II in the low-luminosity host sample (orange) in comparison to those in the high-luminosity host sample (green). The vertical lines indicate the mean for each distribution: pEW(Fe II 5018), pEW(Hα), pEW(Na I D), and pEW(Sc II 6247). The upper and lower panels show the cumulative distributions of each pEW in the two host categories: pEW(Fe II 5018) (upper left), pEW(Hα) (upper right), pEW(Na I D) (lower left), and pEW(Sc II 6247) (lower right). Also shown are the number of events (n), and $\rho_{\rm KS}$.

in lower luminosity hosts display weaker metal lines [specifically pEW(Na I D), pEW(Fe II 5169), pEW(Sc II 6247), pEW(Fe II 5018)]. Given the strong correlation between galaxy stellar mass (or luminosity) and galaxy metallicity, this supports the potential for using SN II spectral diagnostics as proxies for progenitor metallicity. In this section, we compare our results with those found in previous studies to attempt to understand the role of galaxy properties in SN II transient behaviour.

5.1 Comparison to previous studies

Using a sample of 119 events, A16 found no evidence of a metallicity influence in the diversity of SNe II. They examined potential correlations between metallicity and various photometric parameters ($M_V^{\rm max}$, s_2, and OPT$_{\rm d}$), but no significant trend was found.

Employing $P_{\rm d}$ as a proxy for the hydrogen envelope mass, instead of OPT$_{\rm d}$, we similarly find no significant correlations. However, a KS test reject the null hypothesis that both s_2 samples (in high- and low-luminosity hosts) are drawn from parent populations with the same distributions: slower declining SNe II preferentially occur in low-luminosity galaxies. Unlike T16, we do not find a statistically significant difference between the samples when we compare their absolute magnitudes.

Turning to the spectral parameters, A16 found moderate correlations between the pEW(Fe II 5018) and gas-phase metallicity as measured through host H II region emission line analysis. Their results indicate that SNe II with stronger iron lines explode in more metal-rich regions. As we do not have direct metallicity measurements of the SN host galaxies, we instead compare the pEW(Fe II 5018) with the stellar mass of the host galaxy (derived from host photometry) and find a weaker correlation. When A16 use their 'gold' sample (i.e. SNe IIP), their correlations increased. By contrast, in our plateau sample (i.e. SNe II with $s_2 < 1.5$ mag 100 d^{-1}), the correlations are weaker.

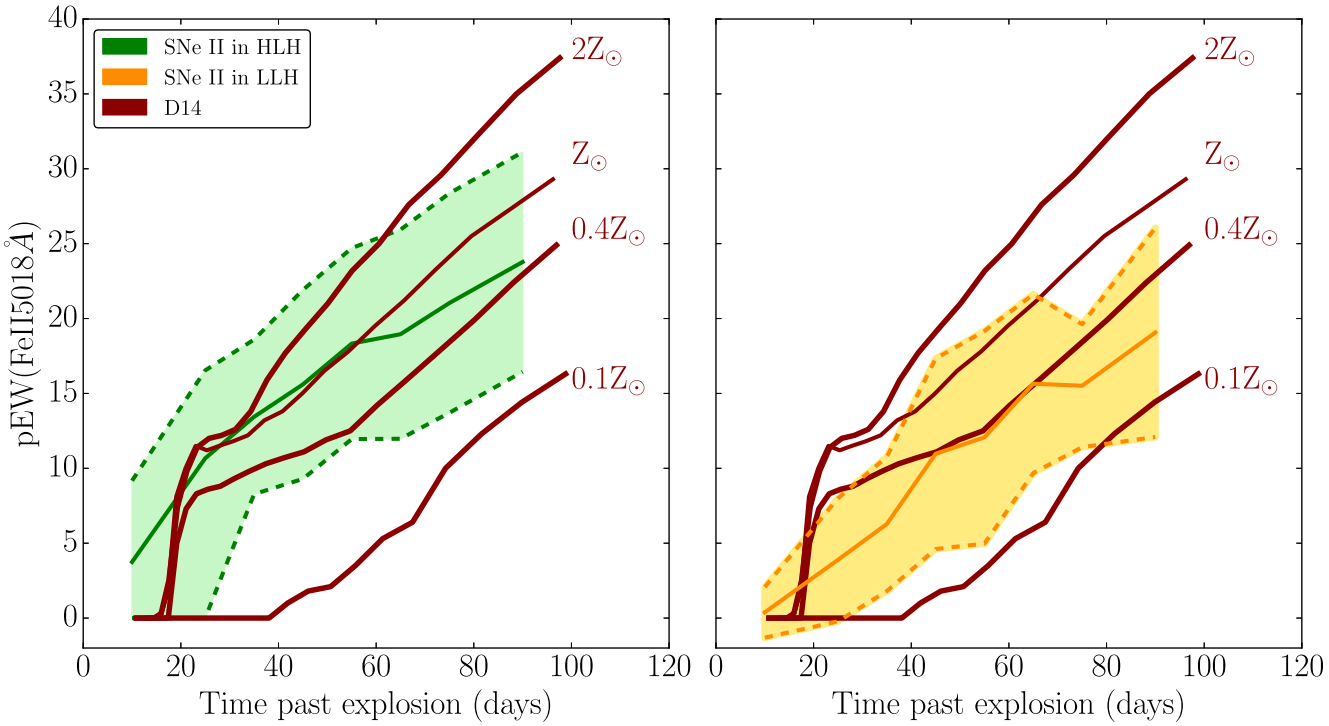

Figure 6. Temporal evolution of pEW(Fe II 5018) from explosion to +90 d, in both the data and models at four different metallicities. The observational data are binned in time. Left: Comparison between the SNe II in high-luminosity hosts. The green solid line represent the mean of the pEW within each time bin, while the dashed green lines indicate the standard deviation. *Right:* The comparison with SNe II in low-luminosity hosts, with the mean of the pEW orange solid line and the standard deviation in dashed orange lines. In both panels, the brown solid lines represent the D14 models as labelled.

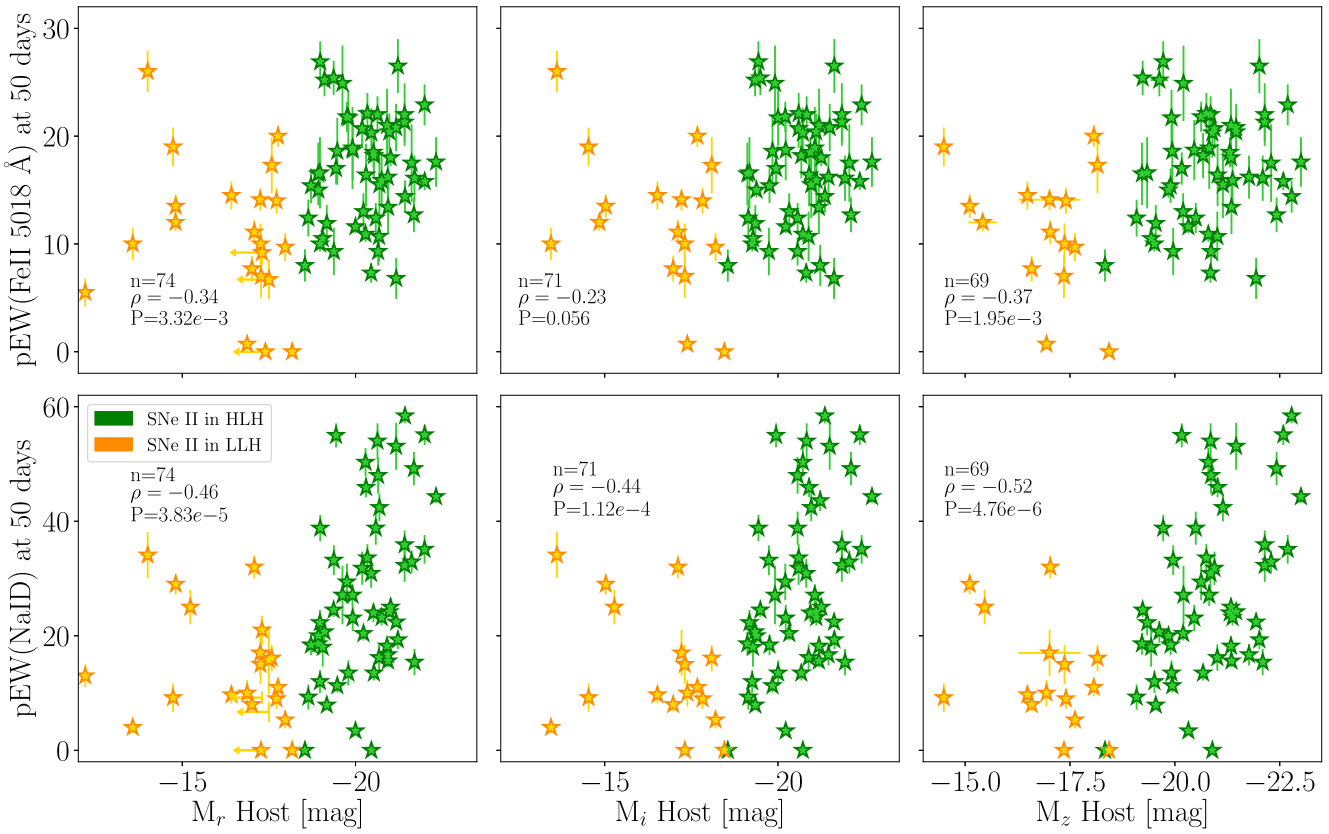

Figure 7. Correlations between pEW(Fe II 5018) (upper panels) and pEW(Na I D) (lower panels), and the galaxy absolute magnitudes: M_r (left), M_i (centre), and M_z (right). Green stars represent SNe in high-luminosity hosts, while yellow stars are SNe II in low-luminosity hosts. In each panel, n is the number of events, ρ is the Pearson's correlation coefficient, and P is the probability of detecting a correlation by chance.

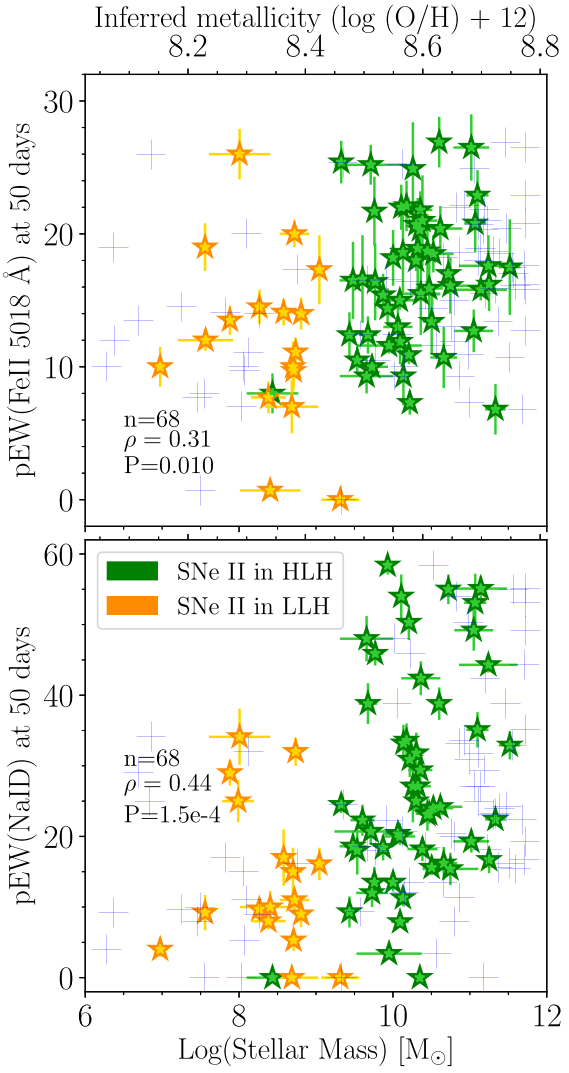

Figure 8. The correlations between pEW(Fe II 5018) and $M_{stellar}$ (upper panel) and between pEW(Na I D) and $M_{stellar}$ (lower panel). Green stars represent SNe II in high-luminosity hosts, while yellow stars are SNe II in low-luminosity hosts. In each panel, n is the number of events, ρ is the Pearson correlation coefficient, and P is the probability of detecting a correlation by chance.

The differences between these two studies are most likely due to the use, in the current study, of integrated stellar mass as a proxy for metallicity, while A16 derived metallicities of host H II regions directly through emission-line spectroscopy. Obtaining such data for our sample will be the focus of a future project.

D14 further found that, in their models, higher metallicity SNe display weaker Hα absorption. Even though the differences in these values are small, they show an opposite behaviour to that found in this work, where SNe II in low-luminosity (low-metallicity) hosts present a lower pEW(Hα). According to D14, the differences in the pEW(Hα) do not originate from metallicity, but are instead probably more sensitive to time dependent effects, density profile, mixing, and clumping.

5.2 Populating the metal-poor region with SNe II

Stoll et al. (2013), D14, and more recently A16 found a lack of SNe II in low-metallicity environments. Although this gap is expected because of an observational bias, some results have shown that SNe II in lower metallicity environments present smaller pEWs of the iron lines and no significant differences in their P_d (A16).

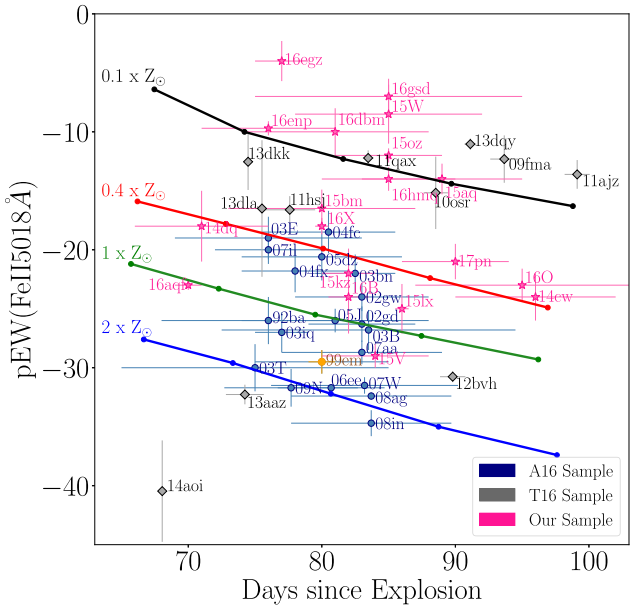

Figure 9. Comparison of the pEW(Fe II 5018) at around 80 d post-explosion between observed and model SN II explosions. In light blue is shown the CSP SNe II with $s_2 < 1.5$ (A16), in grey the (i)PTF sample (T16) and in magenta our SNe II. The solid lines represent the pEW(Fe II 5018) for four different models: 0.1 $Z_\odot$ in black, 0.4 $Z_\odot$ in red, $Z_\odot$ in dark green, and 2 $Z_\odot$ in blue.

T16 showed how the observational gap found in the SN II models at different metallicities was partially filled with their iPTF sample. However, when they compared the pEW(Fe II 5018) with the metallicity of the host galaxy, they found a correlation with a weak significance, which could suggest that the observed lack of SNe II is still visible.

Our sample probes lower luminosity hosts and therefore lower inferred metallicities (Fig. 8). These lower metallicities are also evident when we compare our spectral measurements with the SN models at different metallicities. Reproducing fig. 6 of D14 [the distribution of pEW(Fe II 5018) around 80 d from explosion], it is possible to see how our sample fills the region between 0.1 and 0.4 $Z_\odot$ (Fig. 9). This figure includes the A16 sample, the T16 dataset and our SNe II (magenta). Following the process employed by D14, we measure the pEW for SNe II with available spectra between 65 and 100 d post-explosion. A total of 19 SNe II are incorporated in the pEW distribution plot. From T16, we also select SNe II within this range of time. Fig. 9 shows a significant number of SNe II are consistent with progenitors with a metallicity lower than 0.1 $Z_\odot$.

5.3 Na I D as metallicity indicator?

Recent studies (e.g. A16, T16) have shown the effects of environmental metallicity in the strength of the iron lines in SNe II spectra. However, these studies did not examine the potential influence of metallicity on the strength of other metal lines, such as Sc II, Ba II, Na I D.

Table 7. Pearson correlation coefficients.

Parameter	Host M_B	Host M_r	Host M_i	Host M_z	$M_{\rm stellar}$
$M_V^{\rm max}$	− 0.04 (101; 0.73)	− 0.22 (88; 0.04)	− 0.14 (85; 0.19)	− 0.12 (82; 0.29)	0.19 (82; 0.08)
s_2	− 0.19 (104; 0.06)	− 0.22 (90; 0.04)	− 0.20 (87; 0.07)	− 0.17 (84; 0.11)	0.18 (84; 0.10)
$P_{\rm d}$	− 0.04 (38; 0.81)	− 0.19 (28; 0.32)	− 0.04 (26; 0.84)	0.22 (24; 0.30)	− 0.13 (25; 0.53)
$\rm OPT_d$	0.02 (67; 0.85)	− 0.11 (56; 0.44)	0.03 (54; 0.86)	0.09 (52; 0.52)	0.22 (59; 0.09)
vel(Hα)	− 0.01 (82 0.38)	0.06 (76; 0.59)	0.01 (76; 0.40)	0.05 (74; 0.68)	− 0.08 (69; 0.50)
vel(Hβ)	− 0.08 (83 0.50)	− 0.03 (76; 0.79)	0.01 (76; 0.97)	0.01 (75; 0.91)	− 0.02 (69; 0.84)
vel(Fe II 5018)	− 0.18 (81 0.10)	− 0.23 (72; 0.05)	− 0.13 (72; 0.28)	− 0.12 (71; 0.31)	0.09 (66; 0.49)
vel(Fe II 5169)	− 0.16 (81 0.16)	− 0.21 (72; 0.07)	− 0.10 (72; 0.43)	− 0.09 (71; 0.51)	0.02 (66; 0.86)
vel(Na I d)	− 0.17 (76 0.14)	− 0.07 (69; 0.58)	− 0.09 (67; 0.49)	− 0.52 (65; 0.23)	0.05 (64; 0.65)
vel(Ba II 6142)	− 0.14 (50 0.33)	− 0.05 (41; 0.78)	− 0.06 (42; 0.69)	− 0.03 (41; 0.86)	0.06 (39; 0.73)
vel(Sc II 6247)	− 0.15 (51 0.30)	0.09 (43; 0.58)	0.08 (44; 0.59)	0.12 (43; 0.46)	− 0.05 (40; 0.74)
pEW(Hα)	− 0.19 (79; 0.10)	$-0.32\ (73; 6.51\times10^{-3})$	− 0.29 (70; 0.01)	− 0.27 (68; 0.02)	$0.34\ (67; 4.27\times10^{-3})$
pEW(Hβ)	− 0.08 (81; 0.47)	0.08 (75; 0.52)	− 0.01 (72; 0.94)	0.02 (70; 0.85)	− 0.02 (69; 0.88)
pEW(Fe II 5018)	− 0.13 (80; 0.25)	$-0.34\ (74; 3.32\times10^{-3})$	− 0.23 (71; 0.06)	$-0.37\ (69; 1.96\times10^{-3})$	0.31 (68; 0.01)
pEW(Fe II 5169)	− 0.21 (80; 0.06)	− 0.26 (74; 0.03)	− 0.18 (71; 0.14)	$0.40\ (69; 7.04\times10^{-4})$	0.25 (68; 0.04)
pEW(Na I D)	$-0.49\ (80; 5.00\times10^{-6})$	$-0.44\ (73; 9.72\times10^{-5})$	$-0.44\ (71; 1.13\times10^{-4})$	$-0.52\ (69; 4.76\times10^{-6})$	$0.44\ (68; 1.51\times10^{-4})$
pEW(Ba II 6142)	− 0.27 (77; 0.02)	$-0.33\ (68; 5.33\times10^{-3})$	− 0.31 (67; 0.01)	− 0.30 (65; 0.01)	0.31 (64; 0.01)
pEW(Sc II 6247)	− 0.24 (78; 0.04)	− 0.31 (69; 0.01)	− 0.31 (67; 0.01)	− 0.30 (65; 0.01)	$0.32\ (64; 9.02\times10^{-3})$

Note. The number of events and the probability of finding such correlation by change are presented in parenthesis.

We test the relations between host galaxy properties and the pEW(Hα) absorption component, pEW(Hβ), pEW(Na I D), pEW(Fe II 5018), pEW(Fe II 5169), pEW(Ba II 6142), and pEW(Sc II 6247). We find that, with the exception of Na I d, these lines have only weak correlations with host galaxy properties (see Table 7). The Na I d line shows a significant correlation with host galaxy luminosity and $M_{\rm stellar}$. Fig. 7 and Fig. 8 present these results. Additionally, using the KS test, we also find that Na I D display statistically significant differences between the low- and high-luminosity groups.

This analysis suggests that Na I D may be a good indicator of global properties of the galaxies, such as metallicity. This is surprising as, given the lightness of sodium, significant contamination of the hydrogen envelope with sodium created from nuclear burning during the star's life is expected. These results suggest that either the mixing of such material to the outer envelope is very low, or that the degree of mixing also depends on progenitor metallicity, with higher metallicity progenitors undergoing more vigorous mixing during their lifetimes. However, a theoretical study on the production of sodium in massive stars at difference metallicity is needed in order to understand these results.

6 CONCLUSIONS

In this work, we have presented an analysis of SNe II in low-luminosity galaxies, and compared to those SNe in high-luminosity hosts. A total of 138 SNe II were analysed using spectral diagnostics (velocities and pEWs) and photometric ($M_V^{\rm max}$, s_2, and $P_{\rm d}$) properties, and compared with their host galaxy absolute magnitudes and stellar masses, which we use as a proxy for galaxy metallicity. Our main results are:

(i) We find that SNe II in more metal-rich environments (i.e. a large stellar mass) display stronger metal lines in their photospheric spectra. This is in agreement with the prediction from the models of D14. We found stronger correlations with pEW(Na I D) than with pEW(Fe II 5018).

(ii) There is a commonly held view that the degree of hydrogen-envelope mass-stripping is strongly dependent on progenitor metallicity in single star evolution. We do not detect any signature of this, but it is likely that our RSG progenitors are drawn mostly from the 8–15 $\rm M_\odot$ range due to IMF statistics. At these masses and luminosities, the mass-loss rates on the main sequence are not high enough to have significant effect on the plateau ($\sim$1–2 $\rm M_\odot$ lost; Eldridge & Tout 2004), which is consistent with our measurements.

(iii) We find that all absorption lines in the spectra of SNe II located in low-luminosity galaxies have smaller pEWs than those SNe II in high-luminosity hosts. Comparing these results with models at different metallicities, we found that the Hα absorption feature shows the opposite behaviour. We found weak absorption in SNe II in low-luminosity hosts, while D14 found stronger H α absorption for low-metallicity models.

(iv) We find no evidence that expansion velocities (and therefore explosion energy) are affected by metallicity of the host. This suggests there is physically little difference between the progenitor structure and explosions at low and high metallicity for RSGs that explode as SNe II.

ACKNOWLEDGEMENTS

This work is based (in part) on observations collected at the European Organisation for Astronomical Research in the Southern Hemisphere, Chile as part of PESSTO (the Public ESO Spectroscopic Survey for Transient Objects Survey) ESO program 188.D-3003, 191.D-0935, 191.D-0935, 197.D-1075, 199.D-0143. This work makes use of data from Las Cumbres Observatory, the Supernova Key Project, and the Global Supernova Project. Part of the funding for GROND (Gamma-Ray Burst Optical/Near-Infrared Detector; both hardware as well as personnel) was generously granted from the Leibniz-Prize to Prof. G. Hasinger (DFG grant HA 1850/28-1).

We thank the anonymous referee for the useful suggestions. We are grateful to Andrea Pastorello, José Luis Prieto, Avet Harutyunyan, and R. Mark Wagner for performing some of the observations used in this work.

CPG and MS acknowledge support from EU/FP7-ERC grant no. [615929]. LG was supported in part by the US National Science Foundation under grant AST-1311862. Support for IA was provided by NASA through the Einstein Fellowship Program, grant PF6-170148. T-W Chen acknowledgments the funding provided by the Alexander von Humboldt Foundation. DAH, GH, and CM are supported by NSF grant AST-1313484. GL was supported by a research grant (19054) from VILLUM FONDEN. MG is supported by the Polish National Science Centre grant OPUS 2015/17/B/ST9/03167. Support for FOE is provided by FONDECYT through grant 11170953 and by the Ministry of Economy, Development, and Tourism's Millennium Science Initiative through grant IC120009, awarded to The Millennium Institute of Astrophysics, MAS. Support for GP is provided by the Ministry of Economy, Development, and Tourism's Millennium Science Initiative through grant IC120009, awarded to The Millennium Institute of Astrophysics, MAS. SJS acknowledges funding from ERC grant 291222 and STFC grant ref: ST/P000312/1.

This research has made use of the NASA/IPAC Extragalactic Database (NED) which is operated by the Jet Propulsion Laboratory, California Institute of Technology, under contract with the National Aeronautics. We acknowledge the usage of the HyperLeda database (http://leda.univ-lyon1.fr)

Funding for the Sloan Digital Sky Survey IV has been provided by the Alfred P. Sloan Foundation, the U.S. Department of Energy Office of Science, and the Participating Institutions. SDSS-IV acknowledges support and resources from the Center for High-Performance Computing at the University of Utah. The SDSS web site is www.sdss.org. SDSS-IV is managed by the Astrophysical Research Consortium for the Participating Institutions of the SDSS Collaboration including the Brazilian Participation Group, the Carnegie Institution for Science, Carnegie Mellon University, the Chilean Participation Group, the French Participation Group, Harvard-Smithsonian Center for Astrophysics, Instituto de Astrofísica de Canarias, The Johns Hopkins University, Kavli Institute for the Physics and Mathematics of the Universe (IPMU) / University of Tokyo, Lawrence Berkeley National Laboratory, Leibniz Institut für Astrophysik Potsdam (AIP), Max-Planck-Institut für Astronomie (MPIA Heidelberg), Max-Planck-Institut für Astrophysik (MPA Garching), Max-Planck-Institut für Extraterrestrische Physik (MPE), National Astronomical Observatories of China, New Mexico State University, New York University, University of Notre Dame, Observatário Nacional / MCTI, The Ohio State University, Pennsylvania State University, Shanghai Astronomical Observatory, United Kingdom Participation Group, Universidad Nacional Autónoma de México, University of Arizona, University of Colorado Boulder, University of Oxford, University of Portsmouth, University of Utah, University of Virginia, University of Washington, University of Wisconsin, Vanderbilt University, and Yale University.

The Pan-STARRS1 Surveys (PS1) have been made possible through contributions of the Institute for Astronomy, the University of Hawaii, the Pan-STARRS Project Office, the Max-Planck Society and its participating institutes, the Max Planck Institute for Astronomy, Heidelberg and the Max Planck Institute for Extraterrestrial Physics, Garching, The Johns Hopkins University, Durham University, the University of Edinburgh, Queen's University Belfast, the Harvard-Smithsonian Center for Astrophysics, the Las Cumbres Observatory Global Telescope Network Incorporated, the National Central University of Taiwan, the Space Telescope Science Institute, the National Aeronautics and Space Administration under Grant No. NNX08AR22G issued through the Planetary Science Division of the NASA Science Mission Directorate, the National Science Foundation under Grant No. AST-1238877, the University of Maryland, and Eotvos Lorand University (ELTE).

REFERENCES

Albareti F. D. et al., 2017, ApJS, 233, 25
Anderson J. P. et al., 2014, ApJ, 786, 67
Anderson J. P. et al., 2016, A&A, 589, A110
Anderson J. P. et al., 2018, Nature Astronomy, 2, 574
Arcavi I. et al., 2010, ApJ, 721, 777
Arcavi I. et al., 2012, ApJ, 756, L30
Barbon R., Ciatti F., Rosino L., 1979, A&A, 72, 287
Brown T. M. et al., 2013, PASP, 125, 1031
Buzzoni B. et al., 1984, The Messenger, 38, 9
Chambers K. C. et al., 2016, preprint (arXiv:1612.05560)
Chieffi A., Limongi M., 2013, ApJ, 764, 21
Chun S.-H., Yoon S.-C., Jung M.-K., Kim D. U., Kim J., 2017, ApJ, 853, 79
Dessart L. et al., 2014, MNRAS, 440, 1856
Dessart L., Hillier D. J., Waldman R., Livne E., 2013, MNRAS, 433, 1745
Eldridge J. J., Tout C. A., 2004, MNRAS, 353, 87
Faran T. et al., 2014a, MNRAS, 442, 844
Faran T. et al., 2014b, MNRAS, 445, 554
Fioc M., Rocca-Volmerange B., 1997, A&A, 326, 950
Firth R. E. et al., 2015, MNRAS, 446, 3895
Flewelling H. A. et al., 2016, preprint (arXiv:1612.05243)
Galbany L. et al., 2016, AJ, 151, 33
Goldman S. R. et al., 2017, MNRAS, 465, 403
González-Gaitán S. et al., 2015, MNRAS, 451, 2212
Greiner J. et al., 2008, PASP, 120, 405
Gutiérrez C. P. et al., 2017a, ApJ, 850, 89
Gutiérrez C. P. et al., 2017b, ApJ, 850, 90
Hamuy M. et al., 1993, AJ, 106, 2392
Hamuy M. et al., 2006, PASP, 118, 2
Hamuy M., 2003, ApJ, 582, 905
Heger A., Fryer C. L., Woosley S. E., Langer N., Hartmann D. H., 2003, ApJ, 591, 288
Huang F. et al., 2018, MNRAS,
Krühler T. et al., 2008, ApJ, 685, 376
Landolt A. U., 1992, AJ, 104, 372
Landolt A. U., 2007, AJ, 133, 2502
Le Borgne D., Rocca-Volmerange B., 2002, A&A, 386, 446
Makarov D., Prugniel P., Terekhova N., Courtois H., Vauglin I., 2014, A&A, 570, A13
Minkowski R., 1941, PASP, 53, 224
Mokiem M. R. et al., 2007, A&A, 473, 603
Pastorello A., Ramina M., Zampieri L., Navasardyan H., Salvo M., Fiaschi M., 2003, preprint (arXiv:e-prints)
Pejcha O., Prieto J. L., 2015a, ApJ, 799, 215
Pejcha O., Prieto J. L., 2015b, ApJ, 806, 225
Pignata G., Maza J., Hamuy M., Antezana R., Gonzales L., 2009, Revista Mexicana deAstronomia y Astroffisica Conf. Ser., 35, 317
Popov D. V., 1993, ApJ, 414, 712
Rubin A. et al., 2016, ApJ, 820, 33
Salpeter E. E., 1955, ApJ, 121, 161
Sanders N. E. et al., 2015, ApJ, 799, 208
Schlafly E. F., Finkbeiner D. P., 2011, ApJ, 737, 103
Smartt S. J. et al., 2015, A&A, 579, A40
Smartt S. J., 2015, PASA, 32, e016
Smith J. A. et al., 2002, AJ, 123, 2121
Stoll R., Prieto J. L., Stanek K. Z., Pogge R. W., 2013, ApJ, 773, 12
Sullivan M. et al., 2010, MNRAS, 406, 782
Taddia F. et al., 2016, A&A, 587, L7
Valenti S. et al., 2016, MNRAS, 459, 3939
Vink J. S., de Koter A., Lamers H. J. G. L. M., 2001, A&A, 369, 574
Yaron O., Gal-Yam A., 2012, PASP, 124, 668

[1]*Department of Physics and Astronomy, University of Southampton, Southampton, SO17 1BJ, UK*
[2]*European Southern Observatory, Alonso de Córdova 3107, Casilla 19, Santiago, Chile*
[3]*Unidad Mixta Internacional Franco-Chilena de Astronomía (CNRS, UMI 3386), Departamento de Astronomía, Universidad de Chile, Camino El Observatorio 1515, Las Condes, Santiago, Chile*
[4]*CENTRA, Instituto Superior Técnico - Universidade de Lisboa, Portugal*
[5]*PITT PACC, Department of Physics and Astronomy, University of Pittsburgh, Pittsburgh, PA 15260, USA*
[6]*Department of Astronomy and Astrophysics, University of California, Santa Cruz, CA 95064, USA*
[7]*Department of Physics, University of California, Santa Barbara, CA 93106-9530, USA*
[8]*Las Cumbres Observatory, 6740 Cortona Dr Ste 102, Goleta, CA 93117-5575, USA*
[9]*INAF - Osservatorio Astrofisico di Catania, Via Santa Sofia, 78, I-95123, Catania, Italy*
[10]*Max-Planck-Institut für Extraterrestrische Physik, Giessenbachstraße 1, D-85748, Garching, Germany*
[11]*IAP/CNRS, UMR7095, and Sorbonne Université 98bis, Boulevard Arago, F-75014, Paris, France*
[12]*Warsaw University Astronomical Observatory, Al. Ujazdowskie 4, 00-478 Warszawa, Poland*
[13]*University of North Carolina at Chapel Hill, Campus Box 3255, Chapel Hill, NC 27599-3255, USA*
[14]*Astrophysics Research Centre, School of Mathematics and Physics, Queens University Belfast, Belfast BT7 1NN, UK*
[15]*Dark Cosmology Centre, Niels Bohr Institute, University of Copenhagen, Juliane Maries vej 30, DK-2100 Copenhagen, Denmark*
[16]*Carnegie Observatories, Las Campanas Observatory, Casilla 601, La Serena, Chile*
[17]*Millennium Institute of Astrophysics, Vicuna Mackenna 4860, 7820436 Macul, Santiago, Chile*
[18]*Departamento de Astronomía, Universidad de Chile, Camino el Observatorio 1515, Santiago, Chile*
[19]*Departamento de Ciencias Fisicas, Universidad Andres Bello, Avda. República 252, Santiago, Chile*
[20]*Tuorla Observatory, Department of Physics and Astronomy, University of Turku, Väisäläntie 20, FI-21500 Piikkiö, Finland*
[21]*The Oskar Klein Centre, Department of Astronomy, AlbaNova, SE-106 91 Stockholm, Sweden*
[22]*Center for Interdisciplinary Exploration and Research in Astrophysics CIERA, Department of Physics and Astronomy, Northwestern University, Evanston, IL 60208, USA*
[23]*Department of Physics, University of California, Davis, CA 95616, USA*

This paper has been typeset from a TEX/LATEX file prepared by the author.